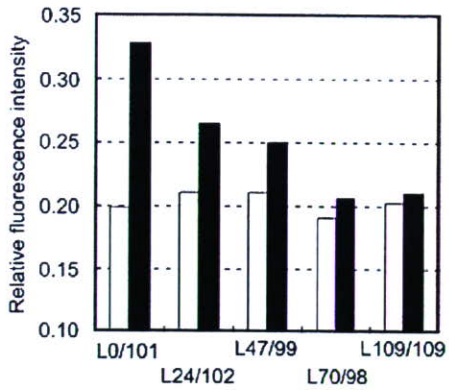


Fig. 7. Tolerability of polyplex micelles against serum incubation evaluated from the fluorescence recovery of the entrapped fluorescein-labeled pDNA due to serum-induced decondensation. Open bars: Fluorescence intensity in 10 mM Tris–HCl (pH 7.4) buffer solution without FBS. Closed bars: Fluorescence intensity after 4 h incubation in the medium containing 90% FBS.

in the transfection medium containing serum due to the strong anchoring of Lys units. This added strength of the Lys anchors is further supported by the sustained fluorescence quenching of fluorescein-labeled pDNA in micelles incubated in 90% FBS for 4 h as seen in Fig. 7. Apparently, fluorescence recovery due to the serum-inducing decondensation of pDNA was progressively inhibited with the increment in the percentage of Lys units in the PEG-*b*-P[Lys/Asp(DET)].

Although the transfection efficacy (Fig. 6) seems to be roughly correlated with the cellular uptake of the micelles (Fig. 5), careful examination reveals the tendency that the PEG-*b*-P[Lys/Asp(DET)] micelles with the lower percentage of Lys units, L24/102, achieved comparable transfection to those with the higher percentage of Lys units, 47/L98 and L70/98, even though the efficacy of pDNA uptake was fairly limited. This tendency becomes more apparent by normalizing the luciferase activity with pDNA uptake (Supplementary Fig. 5). This apparent increase in the transfection efficacy may be explained by the timely release of the loosely associated block catiomers from the micelles in the endosomal compartment to exert a high buffering capacity [9] and their possible interaction with the endosomal membrane component, facilitating the endosomal escape of the complexed pDNA, followed by a smooth release of pDNA directing efficient transcription. The loosely associated nature of L24/102 in the micelle may be supported from a decreased transfection efficacy after serum-preincubation as shown in Fig. 6.

## 4. Conclusion

Polyplex micelles from PEG-*b*-PAsp(DET) revealed a high transfection efficacy to various cell types including primary cells [9–12] presumably due to a low cytotoxicity and a strong pH-buffering capacity. Nevertheless, the weak association power of PAsp(DET) with DNA may be problematic for *in vivo* systemic administration, where the tolerability of polyplexes in proteinaceous media should be a crucial factor. Alternatively, a polylysine has an appreciably high affinity to DNA, however, the transfection efficacy of polylysine polyplexes remains low, possibly due to poor endosomal escaping functions and an impaired release of pDNA from the polyplex with an over-stabilized nature. In this novel study, we sought to alter these discrepancies by placing both Asp(DET) as a buffering unit with low cytotoxicity and Lys as a strong anchoring moiety to DNA in a single polymer strand resulting in PEG-*b*-P[Lys/Asp(DET)]. Polyplexes prepared from pDNA and PEG-*b*-P[Lys/Asp(DET)] have a micellar structure with a PEG palisade, exhibiting a remarkably improved stability compared to PEG-*b*-PAsp(DET)/pDNA polyplex micelles. PEG-*b*-P[Lys/Asp(DET)] polyplex micelles were further revealed to promote cellular internalization, leading to enhanced transfection efficacy even with a subtle excess of block catiomers. This enhanced transfection efficacy could be explained by the synergistic effect of Lys as an anchoring unit and Asp(DET) as a lower toxic endosomal escaping unit. This approach of placing cationic units with discriminating functions, e.g., DNA anchoring and endosomal escaping functions, into a single block catiomer strand is highly promising for future construct designs for effective *in vivo* systemic applications.

## Acknowledgement

This work was financially supported by Research Fellowships of the Japan Society for the Promotion of Science for Young Scientists (JSPS), the Mitsubishi Chemical Corporation Fund, and the Core Research Program for Evolutional Science and Technology (CREST) from the Japan Science and Technology Corporation (JST). The authors express their appreciation to Dr H. Hamada (RIKEN, Japan) for providing the plasmid DNA.

## Appendix A. Supplementary data

Supplementary data associated with this article can be found, in the online version, at doi:10.1016/j.jconrel.2007.06.020.

## References

[1] D.W. Pack, A.S. Hoffman, S. Pun, P.S. Stayton, Design and development of polymers for gene delivery, Nat. Rev. Drug Discov. 4 (2005) 581–593.
[2] E. Mastrobattista, M.A.E.M. van der Aa, W.E. Hennink, D.J.A. Crommelin, Artificial viruses: a nanotechnological approach to gene delivery, Nat. Rev. Drug Discov. 5 (2006) 115–121.
[3] K. Kakizawa, K. Kataoka, Block copolymer micelles for delivery of gene and related compounds, Adv. Drug Deliv. Rev. 54 (2002) 203–222.
[4] K. Itaka, A. Harada, K. Nakamura, H. Kawaguchi, K. Kataoka, Evaluation by fluorescence resonance energy transfer of the stability of nonviral gene delivery vectors under physiological conditions, Biomacromolecules 3 (2002) 841–845.
[5] M. Harada-Shiba, K. Yamauchi, A. Harada, I. Takamisawa, K. Shimokado, K. Kataoka, Polyion complex micelles as a vector in gene therapy-pharmacokinetics and in vivo gene transfer, Gene Ther. 9 (2002) 407–414.
[6] K. Miyata, Y. Kakizawa, N. Nishiyama, Y. Yamasaki, T. Watanabe, M. Kohara, K. Kataoka, Freeze-dried formulations for in vivo gene delivery of PEGylated polyplex micelles with disulfide crosslinked cores to the liver, J. Control. Release 109 (2005) 15–23.
[7] O. Boussif, F. Lezoualc'h, M.A. Zanta, M.D. Mergny, D. Scherman, B. Demeneix, J.-P. Behr, A versatile vector for gene and oligonucleotide transfer into cells in culture and in vivo: Polyethylenimine, Proc. Natl. Acad. Sci. U. S. A. 92 (1995) 7297–7301.

[8] M. Neu, D. Fischer, T. Kissel, Recent advances in rational gene transfer vector design based on poly(ethylene imine) and its derivatives, J. Gene Med. 7 (2005) 992–1009.

[9] N. Kanayama, S. Fukushima, N. Nishiyama, K. Itaka, W.-D. Jang, K. Miyata, Y. Yamasaki, K. Kataoka, PEG-based biocompatible block catiomer with high-buffering capacity for the construction of polyplex micelles showing efficient gene transfer toward primary cells, ChemMedChem 1 (2006) 439–444.

[10] D. Akagi, M. Oba, H. Koyama, N. Nishiyama, S. Fukushima, T. Miyata, H. Nagawa, K. Kataoka, Biocompatible micellar nanovectors achieve efficient gene transfer to vascular lesions without cytotoxicity and thrombus formation, Gene Ther. 14 (2007) 1029–1038.

[11] M. Han, Y. Bae, N. Nishiyama, K. Miyata, M. Oba, K. Kataoka, Transfection study using multicellular tumor spheroids for screening non-viral polymeric gene vectors with low cytotoxicity and high transfection efficiencies, J. Control. Release, in press.

[12] K. Itaka, S. Ohba, K. Miyata, H. Kawaguchi, K. Nakamura, T. Takato, U. Chung, K. Kataoka, Bone regeneration by regulated in vivo gene transfer using biocompatible polyplex nanomicelles, Mol. Ther., in press.

[13] W.H. Daly, D. Poche, The preparation of *N*-carboxyanhydrides of alpha-amino-acids using bis(trichloromethyl)carbonate, Tetrahedron Lett. 29 (1988) 5859–5862.

[14] A. Harada, K. Kataoka, Formation of polyion complex micelles in an aqueous milieu from a pair of oppositely-charged block-copolymers with poly(ethylene glycol) segments, Macromolecules 28 (1995) 5294–5299.

[15] A. Harada, S. Cammas, K. Kataoka, Stabilized α-helix structure of poly (L-lysine)-block-poly(ethylene glycol) in aqueous medium through supramolecular assembly, Macromolecules 29 (1996) 6183–6188.

[16] K. Itaka, K. Yamauchi, A. Harada, K. Nakamura, H. Kawaguchi, K. Kataoka, Polyion complex micelles from plasmid DNA and poly(ethylene glycol)-poly(L-lysine) block copolymer as serum-tolerable polyplex system: physicochemical properties of micelles relevant to gene transfection efficiency, Biomaterials 24 (2003) 4495–4506.

[17] D. Wakebayashi, N. Nishiyama, K. Itaka, K. Miyata, Y. Yamasaki, A. Harada, H. Koyama, Y. Nagasaki, K. Kataoka, Polyion complex micelles of pDNA with acetal-poly(ethylene glycol)-poly(2-(dimethylamino(ethyl methacrylate) block copolymer as the gene carrier system: Physicochemical properties of micelles relevant to gene transfection efficacy, Biomacromolecules 5 (2004) 2128–2136.

CHEMMEDCHEM

DOI: 10.1002/cmdc.200700076

# Enhanced Growth Inhibition of Hepatic Multicellular Tumor Spheroids by Lactosylated Poly(ethylene glycol)-siRNA Conjugate Formulated in PEGylated Polyplexes

Motoi Oishi,[a] Yukio Nagasaki,*[a, c] Nobuhiro Nishiyama,[d] Keiji Itaka,[d] Motoki Takagi,[e] Akira Shimamoto,[e] Yasuhiro Furuichi,[e] and Kazunori Kataoka*[b, d]

*PEGylated polyplexes (lac-PEGylated polyplexes) composed of poly(L-lysine) and lactosylated poly(ethylene glycol)-small interfering RNA conjugate, which inhibits the RecQL1 gene product, were revealed to show an appreciable growth inhibition of multicellular HuH-7 spheroids (human hepatocarcinoma cell lines) for up to 21 days ($IC_{50}$ = 6 nM); this system used as an in vitro three-dimensional (3D) model mimicking the in vivo biology of tumors. The PEGylated polyplexes thus prepared had a size of approximately 110 nm with clustered lactose moieties on their periphery as targeting ligands for the asialoglycoprotein-receptor-expressing HuH-7 cells. In contrast, OligofectAMINE/siRNA (cationic lipoplex) was observed to have almost no growth-inhibitory effect against HuH-7 spheroids, even though the lipoplex showed a stronger growth-inhibitory effect than the lac-PEGylated polyplexes on conventional monolayer-cultured HuH-7 cells. The FITC-tagged conjugate in the lac-PEGylated polyplexes showed smooth penetration into the HuH-7 spheroids compared with that in the lipoplexes, as observed by confocal fluorescence-scanning microscopy. This indicates that the small size of approximately 100 nm and the reduced nonspecific interaction due to the nonionic and hydrophilic lactosylated PEG layer contributes to the smooth penetration of the PEGylated polyplexes into the spheroid interior, eventually facilitating their uptake into the cells composing the spheroids. Cellular apoptosis indicating programmed cell death was also observed in the HuH-7 spheroids treated with the PEGylated polyplexes, revealing that the observed growth inhibition was indeed induced by the RNAi of the RecQL1 siRNA. These data suggest that the smart PEGylated polyplexes can indeed penetrate into the multiple cell layers of 3D tumor masses in vivo, exerting therapeutic effects through the RNAi.*

## Introduction

The targeted delivery of small interfering RNAs (siRNAs)[1] is one of the major challenges in the field of cancer therapy through RNA interference (RNAi),[2] because siRNAs often tend to show low stability against enzymatic degradation, low permeability across the cell membrane, and preferential liver and renal clearance.[3] Therefore, the therapeutic value of siRNAs under in vivo conditions is largely dependent on the development of effective carrier systems which achieve modulated disposition in the body intravenously and accumulation in tumor tissues by enhanced permeability and retention (EPR) effect.[4] A promising strategy in this regard is the combination of PEGylation and carrier, namely a "smart" siRNA carrier (PEGylated polyplex) formulated through the supramolecular assembly (electrostatic interactions) of poly(L-lysine) (PLL) and lactosylated poly(ethylene glycol)-siRNA conjugate (Lac-PEG-siRNA) (Figure 1).[5] These smart PEGylated polyplexes, which have a size of approximately 100 nm, showed the high biocompatibility and enzymatic tolerability due to their segregated polyion complex core surrounded by a palisade of flexible and hydrophilic PEG layers. In particular, these smart PEGylated polyplexes with clustered lactose moieties on their periphery were successfully transported into the monolayer-cultured hepatic tumor cells by mediation of the asialoglycoprotein (ASGP) re-

[a] *Prof. Dr. M. Oishi, Prof. Dr. Y. Nagasaki*
*Tsukuba Research Center for Interdisciplinary Materials Science (TIMS), University of Tsukuba, 1-1-1 Ten-noudai, Tsukuba, Ibaraki 305-8573 (Japan)*
*Fax: (+81) 29-853-5749*
*E-mail: nagasaki@nagalabo.jp*

[b] *Prof. Dr. K. Kataoka*
*Division of Clinical Biotechnology Center for Disease Biology and Integrative Medicine, Graduate School of Medicine, The University of Tokyo, 7-3-1 Hongo, Bunkyo-ku, Tokyo 113-0033 (Japan)*

[c] *Prof. Dr. Y. Nagasaki*
*Master's School of Medical Sciences, Graduate School of Comprehensive Human Sciences, University of Tsukuba, 1-1-1 Ten-noudai, Tsukuba, Ibaraki 305-8573, (Japan)*

[d] *Prof. Dr. N. Nishiyama, Prof. Dr. K. Itaka, Prof. Dr. K. Kataoka*
*Department of Materials Engineering, Graduate School of Engineering, The University of Tokyo, 7-3-1 Hongo, Bunkyo-ku, Tokyo 113-8656 (Japan)*
*Fax: (+81) 3-5841-7139*
*E-mail: kataoka@bmw.t.u-tokyo.ac.jp*

[e] *Dr. M. Takagi, Dr. A. Shimamoto, Dr. Y. Furuichi*
*GeneCare Research Institute Co., Ltd., 200 Kajiwara, Kamakura, Kanagawa 247-0063 (Japan)*

   

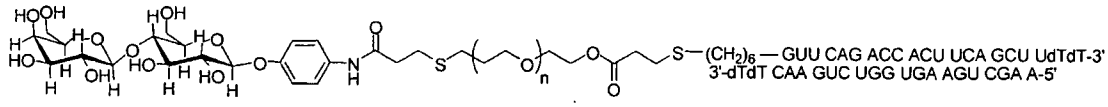


**Figure 1.** Chemical structure of the Lac-PEG-siRNA conjugate.

ceptor, inducing significant gene silencing of firefly luciferase (reporter gene) expression in monolayer-cultured HuH-7 cells at an extremely low siRNA concentration ($IC_{50}$ = 1.3 nM). Therefore, the combination of this smart PEGylated polyplex system and a proper therapeutic siRNA is a promising approach to the creation of a systemic siRNA delivery system for the cancer therapy.

In this regard, siRNA-targeting DNA helicases are of particular interest. DNA helicases have recently been recognized to play important roles in DNA replication, recombination, repair, and transcription. Among many kinds of DNA helicases in living cells, the RecQ helicase family has been shown to have unique properties which are apparently involved in maintaining genomic stability. In humans, the RecQ helicase family has five members: RecQL1, BLM, WRN, RTS, and RecQL5.[6] BLM, WRN, and RTS are causative genes of Bloom syndrome, Werner syndrome, and a subset of Rothmund-Thomson syndrome, respectively, all of which are known to be recessive genetic disorders. Although RecQL1 is not yet known to have a relationship with any human disease, recent findings suggest that it is involved in the maintenance of the human genome.[7] LeRoy et al. have reported that RecQL1 helicase has Holliday junction branch migration activity, and the down-regulation of RecQL1 mRNA by RNAi resulted in an increase in sister chromatid exchange in human cells,[8] suggesting that RecQL1 helicase maintains the human genome by suppressing chromosomal recombination in the S phase. In addition, the RecQL1 protein was up-regulated by mitogenic stimulation or viral transformation in human B-lymphocytes,[9] suggesting that RecQL1 helicase is involved in genomic stabilization in growing cells such as cancer cells. Accordingly, RecQL1 helicase might be a good molecular target in cancer therapy.[10]

We would like to report herein, the significant and prolonged growth inhibition of hepatic multicellular tumor spheroids (MCTSs) by smart PEGylated polyplexes composed of PLL and Lac-PEG-siRNA conjugate bearing a RecQL1-siRNA segment. Note that MCTSs provide an in vivo tumor microenvironment characterized by high cell density, elevated interstitial pressure, hypoxia, and the existence of cell-cell contacts and a tumor extracellular matrix (ECM).[11] Apparently, these environmental factors play key roles in the diffusion, penetration, and growth-inhibitory effects of the siRNA-carriers in solid tumors in vivo. Therefore, using MCTSs, the efficacy of the siRNA delivery systems, including PEGylated polyplexes and lipoplexes, can be simply evaluated from the direct observation of the MCTS size; this method reflects the environmental factors characteristic of tumors and the direct gene silencing ability of the siRNA-carriers.

## Results and Discussion

### Design of the smart PEGylated polyplexes

Our strategy of formulating PEGylated polyplexes is based on the novel conjugation of siRNA with lactosylated PEG (Lac-PEG-siRNA), followed by complexation with poly(L-lysine) (PLL). The PEG-siRNA conjugates were synthesized according to our previously reported method;[5] the Michael addition of α-lactosyl-ω-acryl-PEG toward the 5'-thiol modified sense RNA to obtain Lac-PEG-single stranded RNA conjugate, followed by annealing with antisense RNA to prepare the Lac-PEG-siRNA conjugate through hybridization. A nonlactosylated conjugate, Ace-PEG-siRNA, was also prepared from the α-acetal-ω-acryl-PEG. The lactosyl-(lac-PEGylated polyplex) and nonlactosyl-(ace-PEGylated polyplex) PEGylated polyplexes were then prepared at an N/P ratio of 1 (=[amino group in polycation]/[phosphate group in siRNA segment]) by mixing the siRNA-PEG conjugates and PLL (degree of polymerization (DP) = 40, 100, or 460). The diameter of the PEGylated polyplex was determined to be approximately 110 nm by TEM.[5]

### Growth inhibition of monolayer-cultured tumor cells by the PEGylated polyplexes

The elevation of RecQL1 expression has been positively correlated with various cancer cells, and the depletion of RecQL1 by siRNA complementary to RecQL1 mRNA dramatically inhibited cell proliferation and induced apoptosis in vitro and in vivo.[10] In contrast, the inhibition of the RecQL1 gene product in normal cells by RecQL1 siRNA induces no effect on cell proliferation, suggesting that RecQL1 siRNA is a potential therapeutic tool specific to the molecular targeting of cancer cells. To characterize the growth-inhibitory effect of the PEGylated polyplex system containing RecQL1 siRNA, an MTT assay was done using monolayer-cultured HuH-7 cells (human hepatoma cell) possessing asialoglycoprotein (ASGP) receptors, which recognize and internalize compounds bearing terminal lactose moieties.[12] As seen in Figure 2, almost no growth inhibition was observed for siRNA alone and conjugate alone even at a siRNA concentration of 150 nM in the presence of 10% fetal bovine serum (FBS). On the contrary, lac-PEGylated polyplex with PLL (DP = 100) showed 20% growth inhibition ($P^* < 0.05$) at 150 nM conjugate concentration. These results suggest that the lack of any growth-inhibitory effect on HuH-7 cells for free siRNA and free Lac-PEG-siRNA conjugate may be ascribed to the enzymatic degradation of the siRNA in the medium and to the impaired diffusivity of the negatively charged and hydrophilic free siRNA and Lac-PEG-siRNA conjugate through the negatively charged cell membrane. Significant growth inhibition was observed for the siRNA formulated with commercially

  

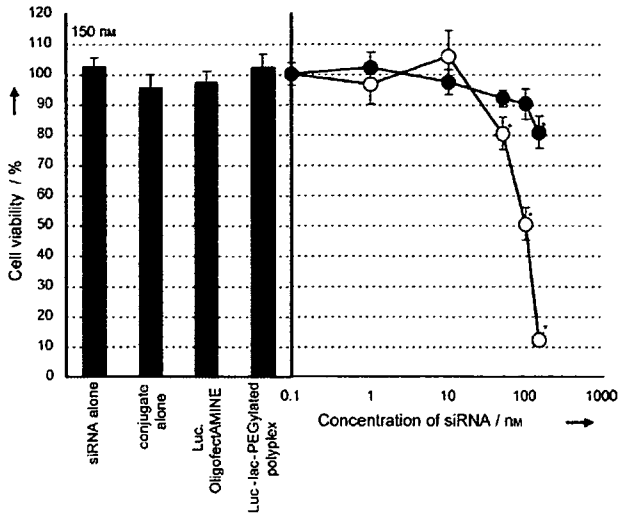


**Figure 2.** Growth inhibitory effect of the lac-PEGylated polyplexes (closed circles) and lipoplexes (open circles) from RecQL1 siRNA on monolayer-cultured HuH-7 cells. The cell viability was determined by means of an MTT assay after 96 h of incubation. The indicated concentrations of siRNA and conjugate are the final ones in the total transfection volume (250 μL). The plotted data are averages of triplicate experiments ± SD. The data points marked with asterisks are statistically significant compared with the mock data (buffer-treated cells) ($P^* < 0.05$).

available cationic lipid reagents, such as OligofectAMINE (lipoplex) (87% inhibition, $P^* < 0.05$). The lipoplex, which is cationic in character, may strongly interact with the negatively charged cell membrane leading to an appreciable increase in cellular uptake. It should be noticed that the lac-PEGylated polyplex and lipoplex, including luciferase-siRNA as a nontargeted sequence, induced no growth inhibition, strongly suggesting that the observed inhibitory effect against monolayer-cultured HuH-7 cells indeed occurred in a sequence-specific manner through RNAi based on the RecQL1-siRNA.

### Growth inhibition of multicellular tumor spheroids (MCTS) by the PEGylated polyplexes

Although the efficacy of the siRNA formulated in the carrier systems in vitro has been generally evaluated by means of monolayer-cultured tumor cells, in vivo results to date have not always been in line with in vitro ones even if the carriers accumulated considerably in the tumor tissues because of the EPR effect. One plausible reason for this discrepancy may be that the monolayer assay only reflects the acute efficacy of the first several days, possibility overlooking the delayed or sustained siRNA action appearing at later stages. Furthermore, the diffusivity of the carriers into the 3D tumor tissue may be crucial in determining the in vivo efficacy, because hypoxic cells that are distant from blood vessels are relatively resistant to chemotherapy, causing the regrowth of the tumor; that is, there are tumor stem cells in the hypoxic regions of some tumors.[13] Therefore, alternatives to in vivo studies (animal experimentations), that is, appropriate in vitro models of in vivo solid tumors, are required to evaluate the prolonged efficacy of siRNA delivery systems, and to properly determine the diffusivity of siRNA-carriers into 3D tumor masses. Worth noting in this regard is the MCTS, which can be maintained in culture medium for many weeks with the physiological characteristics (microenvironment conditions) of in vivo 3D tumor tissues, such as high cell density, elevated interstitial pressure, hypoxia, the existence of cell-cell contacts, and ECM.[11] Indeed, the efficacy of gene delivery by cationic polyplexes and lipoplexes is limited because of their poor penetration ability into MCTSs.[14] Thus, MCTSs were used in this study as 3D in vitro tumor models for screening the growth-inhibitory effect of the siRNAs and their penetration ability into the spheroid interior.

RecQL1 siRNA-mediated growth inhibition of HuH-7 spheroids was assessed under the condition of prolonged culturing (up to 21 days). An HuH-7 spheroid with approximately 100 μm (75–100 μm) in diameter was initially used as the in vitro tumor model, because the maximum distance between the capillary blood vessels within avascular solid tumors is believed to be 200 μm or less.[15] As seen in Figure 3, no growth-inhibitory effect was observed for the siRNA alone or the Lac-PEG-siRNA conjugate alone, even at siRNA concentrations as high as 100 nM. These findings are consistent with the results obtained from the MTT assay using monolayer-cultured HuH-7 cells (Figure 2). In contrast, both the ace-PEGylated and lac-PEGylated polyplexes revealed a significant growth-inhibitory

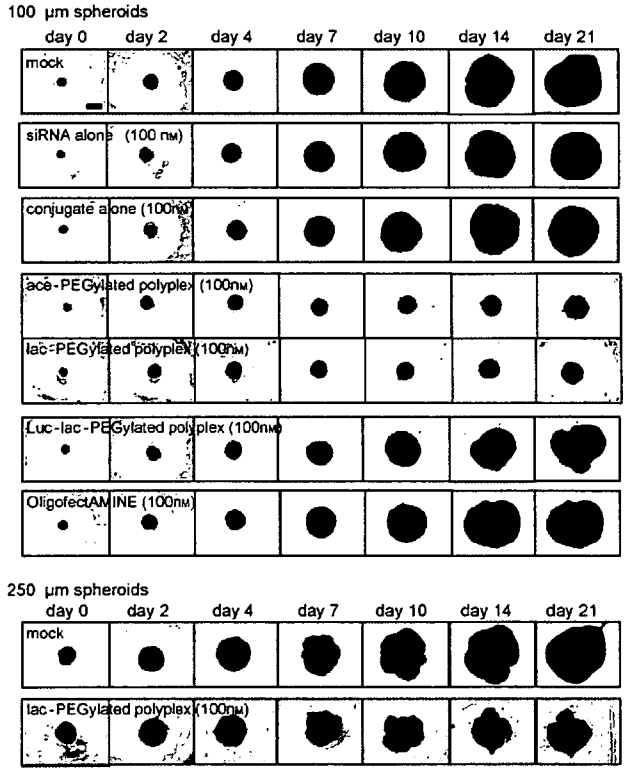


**Figure 3.** Phase-contrast images of the HuH-7 spheroids with an initial diameter of 100 μm and 250 μm (bar = 100 μm) treated with siRNA alone, Lac-PEG-siRNA conjugate alone, ace-PEGylated polyplex, lac-PEGylated polyplex, Luc-lac-PEGylated polyplex, and OligofectAMINE at concentrations of 100 nM.

  

effect in a dose-dependent manner (Figure 4a and b). In particular, the lac-PEGylated polyplexes exerted far more effective growth inhibition than the ace-PEGylated polyplexes at a conjugate concentration of as low as 10 nM; the 50% inhibitory concentration ($IC_{50}$) was determined to be 6 nM and 25 nM for the lac-PEGylated polyplex and ace-PEGylated polyplex, respectively (Figure 5). This almost fourfold increase in the growth-inhibitory effect exerted by lac-PEGylated polyplex is likely to be due to the facilitated uptake into the HuH-7 cells through an ASGP receptor-mediated endocytosis process.[5] This long-term growth-inhibitory effect (up to 21 days) on the spheroids by the single dose of PEGylated polyplexes added at the beginning is worth noting. The control lac-PEGylated polyplex, which included a siRNA against the firefly luciferase sequence (Luc-lac-PEGylated polyplex), induced almost no growth-inhibitory effect even at a conjugate concentration of 100 nM, strongly suggesting that the observed growth-inhibitory effect of the PEGylated polyplexes on the HuH-7 spheroids indeed occurred in a sequence-specific manner (Figure 3 and 4). Although the lipoplexes showed a higher growth-inhibitory effect than the PEGylated polyplex system on monolayer-cultured HuH-7 cells (Figure 2), almost no growth-inhibitory effect on the HuH-7 spheroids was observed even at a siRNA concentration of 100 nM (Figures 3 and 4a). This is presumably due to the cationic nature of the lipoplexes interacting nonspecifically with the negatively charged cell membrane and ECM, which leads to poor penetration into the HuH-7 spheroids. In addition, the spheroid size did not influence the growth-inhibitory effect of the PEGylated polyplexes; the lac-PEGylated polyplexes showed a significant growth-inhibitory effect on the HuH-7 spheroids with an initial diameter of both 200 (data not shown) and 250 μm (Figure 3), whereas the lipoplexes showed almost no growth-inhibitory effect even at high siRNA concentrations (100 nM).

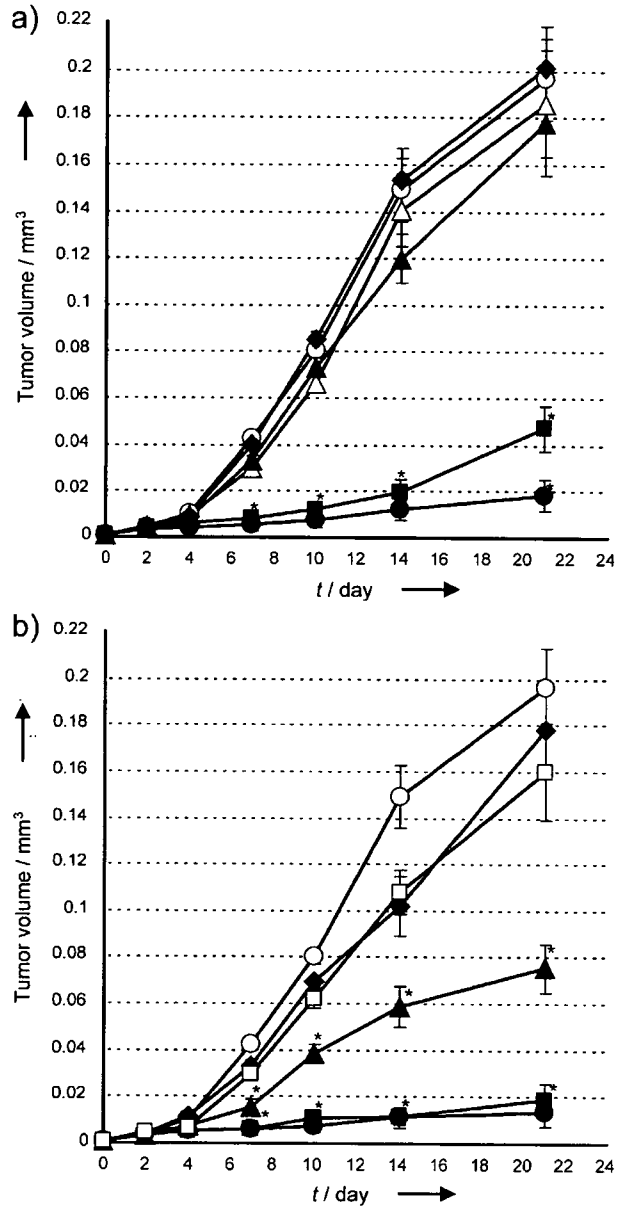


**Figure 4.** Time-dependent change in the volume of the spheroids treated with a) ace-PEGylated polyplexes and b) lac-PEGylated polyplexes; mock (open circles), OligofectAMINE at [siRNA] = 100 nM (open triangles), Luc-lac-PEGylated polyplex at [conjugate] = 100 nM (open squares), and the PEGylated polyplexes at [conjugate] = 100 nM (closed circles), 50 nM (closed squares), 10 nM (closed triangles), and 1 nM (closed lozenges). The volume of the spheroids was calculated as described in the Experimental Section. The data are averages of five HuH-7 spheroids ±SD. The data points marked with asterisks are statistically significant compared with the mock data (buffer-treated cells) ($P^* < 0.05$).

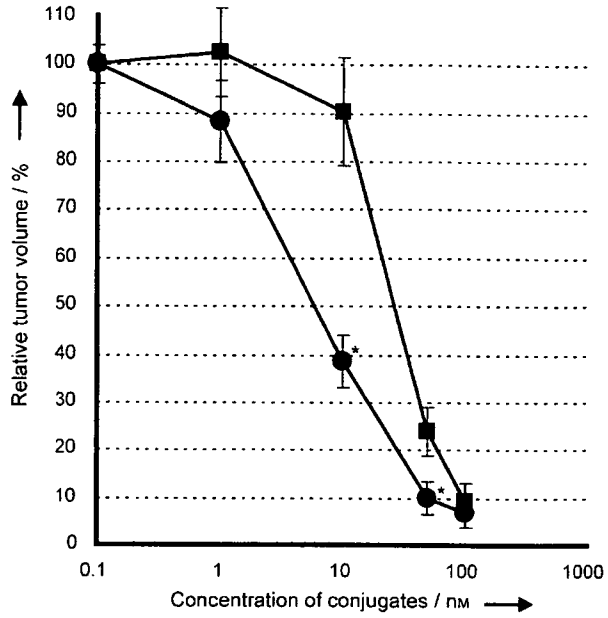


**Figure 5.** Effect of the complexed PEG-siRNA conjugate concentration on the growth inhibition of the HuH-7 spheroids with an initial diameter of 100 μm (closed squares: ace-PEGylated polyplexes; closed circles: lac-PEGylated polyplexes). The relative spheroid volume as the vertical axis was defined as the ratio of volume of the HuH-7 spheroids treated with PEGylated polyplexes to that of the mock sample on day 21. The data are averages of five HuH-7 spheroids ±SD. The data points for the lac-PEGylated polyplexes marked with asterisks are statistically significant compared with those for the ace-PEGylated polyplexes at the corresponding concentrations ($P^* < 0.05$).

  

### Effect of the PLL length on the growth inhibition of spheroids by the PEGylated polyplexes

The effect of the PLL length on the growth inhibition of spheroids induced by the lac-PEGylated polyplexes was then examined. PLLs with varying DPs (40, 100, or 460) were used to prepare the PEGylated polyplex of the PEG-siRNA conjugate. As can be seen in Figure 6a, a striking effect of the PLL length on the growth inhibition of HuH-7 spheroids was observed at a conjugate concentration of 10 nM; the lac-PEGylated polyplexes prepared from shorter PLL (DP = 40) showed only limited efficacy relative to those from longer PLLs (DP = 100 or 460). Consequently, the $IC_{50}$ was determined to be 7 nM, 6 nM, and 70 nM for the lac-PEGylated polyplexes prepared from PLL with DP = 460, DP = 100, and DP = 40, respectively (Figure 6b). These results indicate that the lac-PEGylated polyplexes formed from shorter PLL (DP = 40) are probably unstable under the extremely dilute conditions because of the critical dissociation phenomenon,[16] resulting in the impaired cellular uptake of the Lac-PEG-siRNA conjugate.

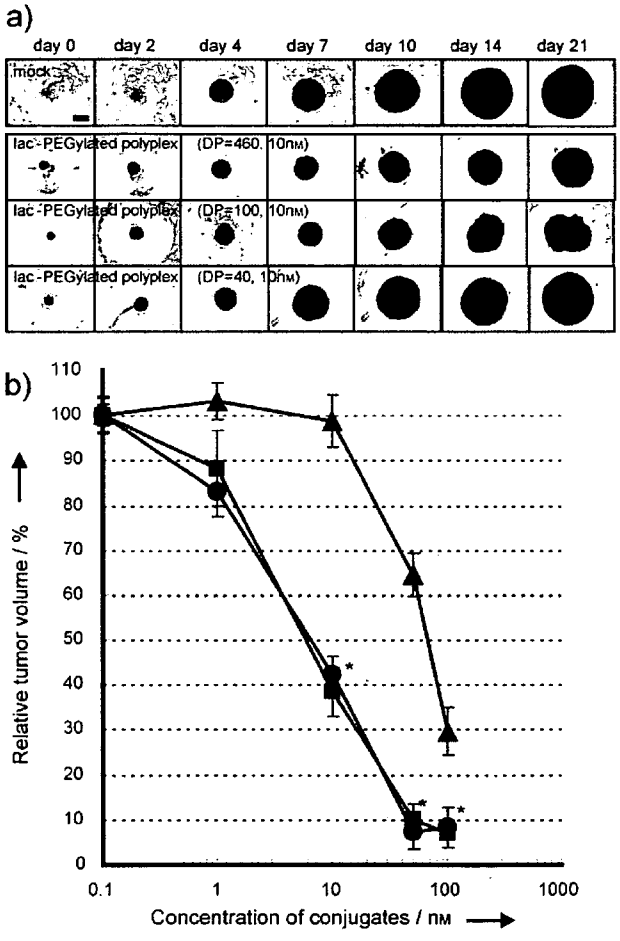


**Figure 6.** Effect of the PLL length on the growth-inhibitory effect of the lac-PEGylated polyplexes on the HuH-7 spheroids with an initial diameter of 100 μm (bar = 100 μm). a) Phase-contrast images of spheroids treated with the lac-PEGylated polyplexes composed of PLL with varying chain lengths. b) Change in the relative volume of the HuH-7 spheroids on day 21 with various concentrations of lac-PEGylated polyplexes composed of PLL with varying chain lengths (closed triangles: DP = 40; closed squares: DP = 100; closed circles: DP = 460). The relative spheroid volume as the vertical axis was defined as the ratio of volume of the HuH-7 spheroids treated with PEGylated polyplexes to that of the mock sample on day 21. The data are averages of five HuH-7 spheroids ± SD. The data points marked with asterisks are statistically significant compared with those for the lac-PEGylated polyplexes (DP = 40) at the corresponding concentrations ($P^* < 0.05$).

### Distribution of the PEGylated polyplexes in multicellular tumor spheroids

To confirm whether or not the lac-PEGylated polyplex can effectively penetrate into the HuH-7 spheroids, 5′-FITC-labeled (fluorescein isothiocyanate) oligodeoxynucleotide (ODN) having the same antisense sequence as the firefly luciferase siRNA was hybridized with the sense firefly luciferase PEG-ODN conjugate to form an FITC-labeled Lac-PEG-dsODN conjugate. The FITC-labeled conjugate was mixed with PLL (DP = 100) at an N/P ratio of 1 to form a PEGylated polyplex with the FITC-label (FITC-PEGylated polyplex). An FITC-labeled lipoplex was also prepared by mixing the OligofectAMINE with FITC-labeled dsODN having the same sequence as the firefly luciferase siRNA. The fluorescence of the FITC-labeled lipoplexes and the FITC-PEGylated polyplexes was observed under a confocal fluorescence-scanning microscope after 48 h of incubation as shown in Figure 7. Most of the fluorescence from the FITC-labeled lipoplexes was seen only at the periphery of the HuH-7 spheroid even after 48 h of incubation (Figure 7a), indicating that the lipoplexes have a poor ability to penetrate into the HuH-7 spheroids, presumably due to the large complex size and the strong interaction with the negatively charged cell membrane and/or ECM.[17] This poor penetration of the lipoplexes into the HuH-7 spheroids obviously has a negative effect on the RecQL1 siRNA-mediated growth inhibition. In sharp contrast, the fluorescence from the FITC-PEGylated polyplexes was observed not only at the periphery but also much

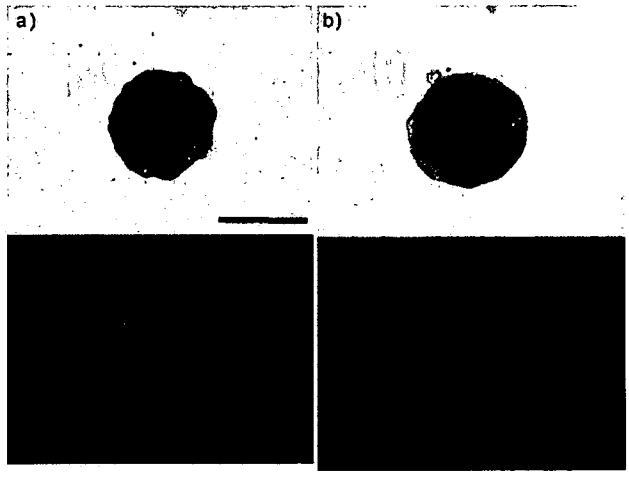


**Figure 7.** Distribution in the HuH-7 spheroids of the a) FITC-labeled dsODN in the OligofectAMINE lipoplexes (z-axis: 87 μm) and b) FITC-labeled Lac-PEG-dsODN conjugate in the lac-PEGylated polyplexes (z-axis: 79 μm) after 48 h of incubation. Initial diameter of the spheroids: 100 μm (bar = 200 μm).

  

farther in the interior of the HuH-7 spheroids (Figure 7b) than that of the FITC-labeled lipoplexes after 48 h of incubation (Figure 7b). This result suggests that the small size of approximately 100 nm and the nonionic and hydrophilic PEG shell of the PEGylated polyplexes may reduce the nonspecific interaction of the micelles with the cell membrane and/or ECM, allowing their smooth penetration into the HuH-7 spheroids.[18]

### Detection of apoptosis in the HuH-7 spheroids

To confirm whether or not the observed growth-inhibitory effect of the PEGylated polyplexes on the HuH-7 spheroids is due to the induction of cell death, a Live/Dead staining assay was carried out for the HuH-7 spheroids treated with mock, lipoplex (100 nM), and lac-PEGylated polyplex (50 nM), respectively. By means of confocal fluorescence-scanning microscopy, living and dead cells in the HuH-7 spheroids were individually detected as green fluorescence and red fluorescence, respectively. As can be seen in Figure 8, cell death at the center of the mock-treated HuH-7 spheroid was clearly observed on day 7, whereas living cells were only observed at the periphery of the spheroid. The observed cell death in the mock-treated sample was apparently due to necrosis resulting from the insufficient supply of oxygen and nutriment to the spheroid interior, deficiencies which become significant with increasing spheroid size.[11] Note that the spheroids treated with the lipoplexes showed some zones at the periphery containing dead cells on day two, yet after ten days the distribution of dead and living cells was the same as in the mock-treated samples. In contrast, the spheroids treated with lac-PEGylated polyplexes showed continuous cell death at the periphery even after day ten, resulting in the significant death of cells in the spheroids.

In addition to the Live/Dead staining assay, we performed the detection of activated caspase-3 in the HuH-7 spheroids to confirm the induction of apoptosis. The activation of caspase-3 is known to play a central role in the induction of the apoptosis;[19] therefore, caspase-3 is an appropriate marker for measuring apoptosis induced by RecQL1 siRNA. Activated caspase-3 was detected using Magic Red fluorescence probe (MR-$(DEVD)_2$). In the presence of activated caspase-3, the DEVD amino-acid sequence in the MR-$(DEVD)_2$ is cleaved to generate a red fluorescence.[20] As can be seen in Figure 9, apoptotic cells (fluorescence signals) were not observed in the mock-treated spheroids. In contrast, apoptotic cells (fluorescent signals) were observed at the periphery of the spheroids treated with the lipoplex as early as day one. Nevertheless, there was no sign of apoptosis after seven days. It is worth noting that the apoptotic cells were also observed at the periphery of spheroids treated with the lac-PEGylated polyplex, and the number of apoptotic cells increased with prolonged incubation time, from day four to day ten. Note that apoptotic cells were still observed even after ten days. Other spheroids treated with the lac-PEGylated polyplex also showed a similar tendency. These results strongly suggest that the observed growth-inhibitory effect and cell death in the spheroids treated with PEGylated polyplexes are likely to be due to apoptosis induced by RecQL1 siRNA in the long term. In addition, the significant difference in the observation period for apoptotic cells between the PEGylated polyplexes and the lipoplexes may be ascribed to the lower tolerance of the lipoplexes for the culture environment than the PEGylated polyplexes. The appreciable stability under physiological conditions and the uniform size of 100 nm of the PEGylated polyplexes may contribute to their smooth penetration into the spheroids, eventually facilitating the RNAi effect through the continuous uptake into the tumor cells located in the interior and the periphery of the spheroids.

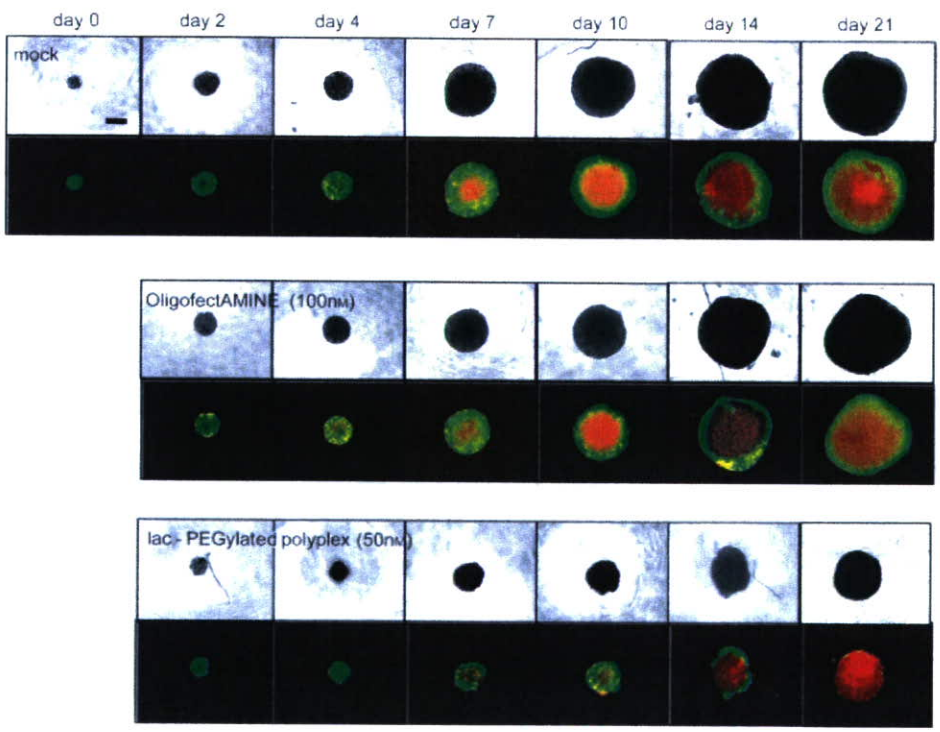


**Figure 8.** Live/Dead staining assay of the HuH-7 spheroids treated with mock, OligofectAMINE ([siRNA] = 100 nM) and lac-PEGylated polyplexes ([conjugate] = 50 nM) (bar = 100 μm). Living and dead cells emit green and red fluorescences, respectively.

## Conclusions

In conclusion, we have demonstrated that MCTSs are useful for evaluating the long-term (up to 21 days) efficacy of siRNA delivery systems (therapeutic value). Note that MCTSs are a versatile in vitro model which can be

  

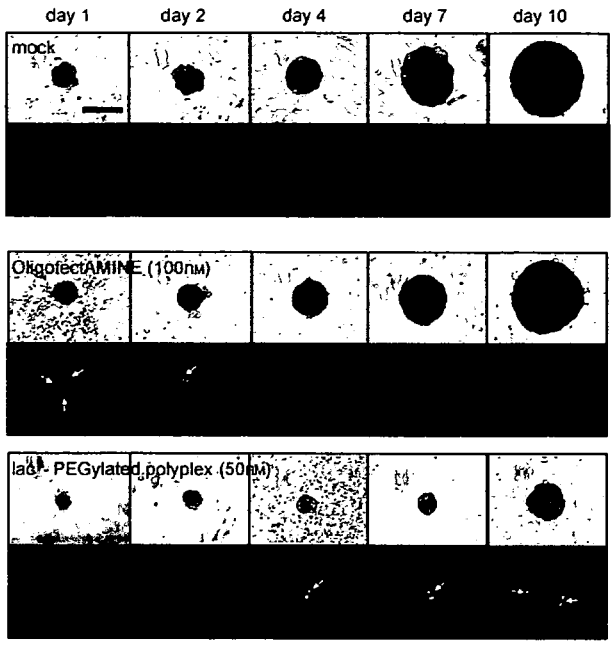


**Figure 9.** Detection of the activated caspapase-3 as the signal of apoptosis in the HuH-7 spheroids treated with mock, OligofectAMINE ([siRNA] = 100 nM), and lac-PEGylated polyplexes ([conjugate] = 50 nM) (bar = 200 μm).

used to estimate the penetration of carriers into 3D tumor tissues and the effect of the ECM and cell-cell contacts (microenvironment) that could otherwise only be examined in vivo using animal models. Indeed, the lac-PEGylated polyplexes composed of the Lac-PEG-siRNA conjugate and PLL showed a remarkable growth-inhibitory effect ($IC_{50}$ = 6 nM) on the HuH-7 spheroids, inducing long-term apoptotic cell death by means of RecQL1 siRNA. Several important factors are likely to be synergistically involved in the pronounced growth-inhibitory effect of the PEGylated polyplexes, such as the improvement of the stability against enzymatic degradation, smooth penetration into the spheroid interior, and enhancement of the cellular uptake through ASGP receptor-mediated endocytosis. In sharp contrast, the lipoplexes showed almost no growth-inhibitory effect even at a siRNA concentration 100 nM in the HuH-7 spheroids, presumably due to the poor penetration into the spheroids. Furthermore, spheroids derived directly from patients' tumor tissues offer the opportunity of studying the efficacy of delivery systems in the unique tumor cell microenvironments characteristic to individual patients. Thus, MCTSs, as an in vitro tumor model, are expected to be useful in the assessment of the usefulness of siRNA carrier systems in tumor targeting.

## Experimental Section

**Materials:** PLLs (degree of polymerization (DP) = 40, $M_w$ = 8300; DP = 100, $M_w$ = 20900; DP = 460, $M_w$ = 75900) were purchased from Sigma. OligofectAMINE and LipofectAMINE were purchased from Invitrogen. 5'-Thiol-modified sense RNAs (HS-$(CH_2)_6$-CUU ACG CUG AGU ACU UCG AdTdT-3', firefly luciferase, pGL3-control sense sequence[1] and HS-$(CH_2)_6$-GUU CAG ACC ACU UCA GCU UdTdT-3', RecQL1, sense sequence[10]) and unmodified antisense RNA (5'-UCG AAG UAC UCA GCG UAA GdTdT-3', firefly luciferase, pGL3-control antisense sequence and 5'- AAG CUG AAG UGG UCU GAA CdTdT-3', RecQL1, antisense sequence) were purchased from Dharmacon. Water was purified using a Milli-Q instrument (MILLIPORE). Plasmid DNAs (pDNA) encoding firefly luciferase (pGL3-Control, Promega; 5256 bp) and renilla luciferase (pRL-TK, Promega; 4045 bp) were amplified using EndoFree Plasmid Maxi or Mega Kits (QIAGEN). The DNA concentration was determined by reading the absorbance at 260 nm. A spheroid culture plate, Celltight Spheroid Culture Plate, was purchased from Sumitomo Bakelite. MTT assay reagents and a double staining kit (Live/Dead assay) were purchased from DOJINDO. A Magic Red Caspase Detection Kit was purchased from Immunochemistry Technologies.

**Preparation of the PEGylated polyplexes:** The PEG-siRNA conjugates were prepared as described in the previous report.[5] Specific amounts of the PEG-siRNA conjugate (50 μM) and PLL were separately added to 10 mM Tris-HCl buffer (pH 7.4) to prepare the 10 μM stock solutions. The solutions were filtered through a 0.1 μm filter to remove the dust. The PEG-siRNA conjugate in 10 mM Tris-HCl buffer (pH 7.4) was mixed with PLL stock solution in 10 mM Tris-HCl buffer (pH 7.4) at an equal unit molar ratio of phosphate groups in the PEG-siRNA conjugate to amino groups in PLL (N/P = 1), followed by the addition of 10 mM Tris-HCl buffer (pH 7.4), adding 0.3 M NaCl to adjust the ionic strength of the solution to the physiological condition (0.15 M NaCl).

**Cell culture:** HuH-7 human cancer cells, derived from a hepatocarcinoma cell line, were obtained from the Cell Resource Center for Biomedical Research, Institute of Development, Aging, and Cancer, Tohoku University. The monolayer-cultured cells and multicellular spheroids were grown in Dulbecco's modified Eagle's medium (DMEM) supplemented with 10% FBS, 100 units/mL penicillin, and 100 μg $mL^{-1}$ streptomycin at 37°C in a humidified 5% $CO_2$ atmosphere.

**MTT assay:** HuH-7 cells were plated in a 96-well plate ($10^4$ cells/well) to allow them to reach about 50% confluence after 24 h and the medium was then changed to fresh DMEM with 10% FBS (180 μL/well). To each well, appropriate amounts of sample were added in 20 μL aliquot. After 48 h of incubation, fresh medium (100 μL/well) was added, and further incubation was carried out for 48 h. The metabolic activity of each well was determined by an MTT assay. The optical absorbance was measured at 560 nm using a microplate reader and converted to the percentage relative to that for mock cells (buffer-treated cells).

**Growth inhibition of the HuH-7 spheroids:** Single-cell suspensions were obtained by the trypsinization of monolayer-cultured HuH-7 cells: 45 μL of single-cell suspensions (80 cells) were seeded in individual wells of a 96-well Celltight Spheroid Culture Plate to form the 100 μm HuH-7 spheroids. After 24 h, the PEGylated polyplexes (N/P = 1), siRNA, Lac-PEG-siRNA conjugate or OligofectAMINE/siRNA (5 μL/well) were added to the well at the prescribed concentration on day 0. Fresh DMEM with 10% FBS was added to each wells on day 2 (25 μL/well), 7 (50 μL/well), 10 (50 μL/well), and 14 (50 μL/well), compensating for the decrease in the medium volume due to the natural evaporation. The perpendicular diameters of the HuH-7 spheroids were measured by means of phase-contrast microscope (Olympus IX71) on day 0, 2, 4, 7, 10, 14, and 21. The volume of the HuH-7 spheroids was calculated using the following formula:[21]

$$4\pi a^2 b/3 = \text{Tumor Volume (mm}^3\text{)}, \quad (1)$$

  

where *a* and *b* are the smallest and largest radius (mm) of the HuH-7 spheroids, respectively.

**Distribution study of FITC-labeled oligodeoxynucleotide in the HuH-7 spheroids:** 5'-FITC-labeled (fluorescein isothiocyanate) oligodeoxynucleotide (ODN) having the same antisense sequence as the firefly luciferase siRNA was hybridized with the sense firefly luciferase PEG-ODN conjugate to form an FITC-labeled Lac-PEG-dsODN conjugate. The lac-PEGylated polyplex was then prepared by mixing FITC-labeled Lac-PEG-dsODN conjugate with PLL (DP = 100). FITC-labeled dsDNA/OligofectAMINE was also prepared as the control. FITC-PEGylated polyplexes or FITC-dsODN/OligofectAMINE were added to the 100 μm HuH-7 spheroids at conjugate or siRNA concentration of 400 nM, and incubated for 48 h. After the incubation, the HuH-7 spheroids were washed three times with phosphate-buffered saline (PBS) and imaged directly in the cell culture medium using a confocal fluorescence-scanning microscope (Olympus IX71 equipped with a confocal IX2-DSU system and an appropriate filter).

**Live/Dead staining assay:** A Live/Dead staining assay was carried out using a double staining kit. The staining solution (15 μL) containing calcein-acetoxymethyl (10 μM) and propidium iodide (30 μM) were added to the HuH-7 spheroids (100 μm initial diameter) treated with the lac-PEGylated polyplexes (50 nM), OligofectAMINE/siRNA (100 nM), or mock on day 0, 2, 4, 7, 10, 14, and 21. After 2 h of incubation, the HuH-7 spheroids were washed three times with PBS and imaged directly in the cell culture medium using a confocal fluorescence-scanning microscope (Olympus IX71 equipped with a confocal IX2-DSU system and an appropriate filter).

**Detection of apoptosis:** The detection of apoptosis was carried out using a Magic Red Caspase Detection Kit. Staining solution (5 μL) containing MR-$(DEVD)_2$ (30 μM) were added to the HuH-7 spheroids (100 μm initial diameter) treated with the lac-PEGylated polyplexes (50 nM), OligofectAMINE/siRNA (100 nM) or mock on day 0, 1, 2, 4, 7, 10, 14, and 21. After 2 h of incubation, the HuH-7 spheroids were washed three times with PBS and imaged directly in the cell culture medium using a confocal fluorescence-scanning microscope (Olympus IX71 equipped with a confocal IX2-DSU system and an appropriate filter).

## Acknowledgements

*This study was partially supported by the Core Research for Evolutional Science and Technology (CREST) program of the Japan Science and Technology Agency (JST) and by the Cell Science Research Foundation.*

**Keywords:** antitumor agents · bioconjugates · drug delivery · siRNA · spheroids

[1] S. M. Elbashir, J. Harborth, W. Lendeckel, A. Yalcin, K. Weber, T. Tuschl, *Nature* **2001**, *411*, 494.
[2] A. Fire, S. Xu, M. K. Montgomery, S. A. Kostas, S. E. Driver, C. C. Mello, *Nature* **1998**, *391*, 806.
[3] D. A. Braasch, Z. Paroo, A. Constantiescu, G. Ren, O. K. Oz, R. P. Mason, D. R. Corey, *Bioorg. Med. Chem. Lett.* **2004**, *14*, 1139.
[4] a) R. M. Schiffelers, A. Ansari, J. Xu, Q. Zhou, Q. Tang, G. Storm, G. Molema, P. Y. Lu, P. V. Scaria, M. C. Woodle, *Nucleic Acids Res.* **2004**, *32*, e149; b) J. Yano, K. Hirabayashi, S. Nakagawa, T. Yamaguchi, M. Nogowa, I. Kashimori, H. Naito, H. Kitagawa, K. Ishiyama, T. Ohgi, T. Irimura, *Clin. Cancer Res.* **2004**, *10*, 7721; c) C. N. Landen, Jr., A. Chavez-Reyes, C. Bucana, R. Schmandt, M. T. Deavers, G. Lopez-Berestein, A. K. Sood, *Cancer Res.* **2005**, *65*, 6910; d) S. Hu-Lieskovan, J. D. Heidel, D. W. Bartlett, M. E. Davis, T. J. Triche, *Cancer Res.* **2005**, *65*, 8984.
[5] M. Oishi, Y. Nagasaki, K. Itaka, N. Nishiyama, K. Kataoka, *J. Am. Chem. Soc.* **2005**, *127*, 1624.
[6] Y. Furuichi, *Ann. N. Y. Acad. Sci.* **2000**, *928*, 121.
[7] a) K. M. Doherty; S. Sharma, L. A. Uzdilla, T. M. Wilson, S. Cui, A. Vindigni, R. M. Brosh, Jr., *J. Biol. Chem.* **2005**, *280*, 28085; S. Sharma, L. A. Uzdilla, T. M. Wilson, S. Cui, A. Vindigni, R. M. Brosh, Jr., *J. Biol. Chem.* **2005**, *280*, 28085; b) S. Sharma, J. A. Sommers, S. Choudhary, J. K. Faulkner, S. Cui, L. Andreoli, L. Muzzolini, A. Vindigni, R. M. Brosh, Jr., *J. Biol. Chem.* **2005**, *280*, 28072.
[8] G. LeRoy, R. Carroll, S. Kyin, M. Seki, M. D. Cole, *Nucleic Acids Res.* **2005**, *33*, 6251.
[9] T. Kawabe, N. Tsuyama, S. Kitao K. Nishikawa, A. Shimamoto, M. Shiratori, T. Matsumoto, K. Anno, T. Sato, Y. Mitsui, M. Seki, T. Enomoto, M. Goto, N. A. Ellis, T. Ide, Y. Furuichi, M. Sugimoto, *Oncogene* **2000**, *19*, 4764.
[10] M. Takagi, A. Shimamoto, Y. Furuichi, A. Sato, WO/2004100990, **2004**.
[11] a) A. Moscona, *Proc. Natl. Acad. Sci. USA* **1957**, *43*, 184; b) R. M. Sutherland, *Science* **1988**, *240*, 177; c) M. T. Santini, G. Rainaldi, P. L. Indovina, *Int. J. Radiat. Biol.* **1999**, *75*, 787.
[12] G. Y. Wu, C. H. Wu, *Adv. Drug Delivery Rev.* **1998**, *29*, 243.
[13] a) J. E. Moulder, S. Rockwell, *Cancer Metastasis Rev.* **1987**, *5*, 313; b) A. L. Harris, *Nat. Rev. Cancer* **2002**, *2*, 38; c) M. Dean, T. Fojo, S. Bates, *Nat. Rev. Cancer* **2005**, *5*, 275.
[14] H. R. Mellor, L. A. Davies, H. Caspar, C. R. Pringle, S. C. Hyde, D. R. Gill, R. Callaghan, *J. Gene Ther.* **2006**, *8*, 1160.
[15] M. A. Konerding, E. Fait, A. Gaumann, *Br. J. Cancer* **2001**, *84*, 1354.
[16] M. Oishi, F. Nagastugi, S. Sasaki, Y. Nagasaki, K. Kataoka, *ChemBioChem* **2005**, *6*, 718.
[17] R. Parthasarathy, P. G. Sscks, D. Harris, H. Brock, K. Mehta, *Cancer Chemother. Pharmacol.* **1994**, *34*, 527.
[18] Y. Bae, N. Nishiyama, S. Fukushima, H. Koyama, Y. Matsumura, K. Kataoka, *Bioconjugate Chem.* **2005**, *16*, 122.
[19] N. A. Thornberry, *Chem. Biol.* **1998**, *5*, R97.
[20] N. A. Thornberry, T. A. Rano, E. P. Peterson, D. M. Rasper, T. Timkey, M. Gracia-Calvo, V. M. Houtzager, P. A. Nordstrom, S. Roy, J. P. Vaillancourt, K. T. Chapman, D. W. Nicholson, *J. Biol. Chem.* **1997**, *272*, 17907.
[21] T. Fujiwara, E. A. Grimm, T. Mukhopadhyay, D. W. Cai, L. B. Owen-Schaub, J. A. Roth, *Cancer Res.* **1993**, *53*, 4129.

Received: April 2, 2007
Revised: April 30, 2007
Published online on June 4, 2007

  

# Dendrimer Generation Effects on Photodynamic Efficacy of Dendrimer Porphyrins and Dendrimer-Loaded Supramolecular Nanocarriers

Yuan Li,[†] Woo-Dong Jang,*[,‡] Nobuhiro Nishiyama,[§] Akihiro Kishimura,[†,+,@] Satoko Kawauchi,[∥] Yuji Morimoto,[∥] Sayaka Miake,[⊥] Takashi Yamashita,[⊥] Makoto Kikuchi,[∥] Takuzo Aida,[#,@] and Kazunori Kataoka*[,†,§,+,@]

*Department of Materials Engineering, Graduate School of Engineering, The University of Tokyo, 7-3-1 Hongo, Bunkyo-ku, Tokyo 113-8656, Japan, Department of Chemistry, College of Science, Yonsei University, 134 Sinchondong, Seodaemun-gu, Seoul 120-749, Korea, Center for Disease Biology and Integrative Medicine, Graduate School of Medicine, The University of Tokyo, 7-3-1 Hongo, Bunkyo-ku, Tokyo 113-0033, Japan, Department of Medical Engineering, National Defense Medical College, 3-2 Namiki, Tokorozawa, Saitama 359-8513, Japan, Department of Pure and Applied Chemistry, Faculty of Science and Technology, Tokyo University of Science, 2641 Yamazaki, Noda-shi, Chiba 278-8510, Japan, Department of Chemistry and Biotechnology, Graduate School of Engineering, The University of Tokyo, 7-3-1 Hongo, Bunkyo-ku, Tokyo 113-8656, Japan, Core Research for Evolutional Science and Technology (CREST), Japan Science and Technology Agency (JST), and Center for NanoBio Integration, The University of Tokyo, 7-3-1 Hongo, Bunkyo-ku, Tokyo 113-8656, Japan*

*Received May 29, 2007. Revised Manuscript Received July 17, 2007*

A series of poly(benzyl ether) dendrimer porphyrins (DPs) (G*n* = *n*-generation dendrimer, *n* = 1–3) was examined as potential photosensitizers for photodynamic therapy (PDT). Polyion complexes (PICs) between the DPs and poly(ethylene glycol)-*block*-poly(L-lysine) (PEG-*b*-PLL) were formed via an electrostatic interaction between the positively charged poly(L-lysine) (PLL) segment and negatively charged periphery of the DPs. Dynamic light scattering (DLS) measurements and transmission electron microscopy (TEM) showed that G3 formed a core–shell-type nanocarrier micelle, whereas G1 and G2 formed irregular-shaped nanoparticles with a relatively high polydispersity. The photophysical properties of the DP-loaded PIC nanocarriers strongly depend on the generation of the DPs. In the case of G1 and G2, their fluorescence lifetime and oxygen consumption ability were significantly reduced by the formation of the PIC nanocarriers, whereas the G3-loaded PIC nanocarrier exhibited almost comparable fluorescence lifetimes and oxygen consumption abilities to the free G3. The incorporation of DPs into PIC nanocarriers resulted in an appreciable increase in the cellular uptake, yet inversely correlated with the generation. Alternatively, the photocytotoxicity of the DPs within the nanocarriers increased with an increase in the generation despite a decrease in the cellular uptake. By correlating the effects of the uptake amount with the photocytotoxicity, the PIC nanocarriers showed remarkable enhancement of the PDT efficacy dependent on the generation of DPs.

## Introduction

Dendrimers with predictable three-dimensional architectures are currently undergoing fast growth in various applications. This is due in part to the variety of applications being pursued for dendrimers.[1,2] In particular, application of dendrimers to biomedical uses has attracted much attention due to the tunable properties of the dendrimer generation, terminal groups, and inner cavity for the incorporation of a variety of molecules.[1–6] PAMAM dendrimers, for example, have been comprehensively investigated as diagnostic tools and drug carriers.[6–8] Recently, we have reported the third generation poly(benzyl ether) dendrimer porphyrins (DPs) as an effective photosensitizer for photodynamic therapy (PDT).[9–11]

PDT involves the administration of a photosensitizer, which preferentially accumulates in target tissues. Subsequent

* To whom correspondence should be addressed. Phone: +81-3-5841-7138. Fax: +81-3-5841-7139. E-mail: kataoka@bmw.t.u-tokyo.ac.jp.
† Department of Materials Engineering, The University of Tokyo.
‡ Yonsei University.
§ Center for Disease Biology and Integrative Medicine, The University of Tokyo.
∥ National Defense Medical College.
⊥ Tokyo University of Science.
# Department of Chemistry and Biotechnology, The University of Tokyo.
+ CREST.
@ Center for NanoBio Integration, The University of Tokyo.

(1) *Dendrimers and other Dendritic Polymers*; Fréchet, J. M. J., Tomalia, D. A., Eds.; John Wiley & Sons: New York, 2001.
(2) Bosman, A. W.; Janssen, H. M.; Meijer, E. W. *Chem. Rev.* **1999**, *99*, 1665–1688.
(3) Lee, I.; Athey, B. D.; Wetzel, A. W.; Meixner, W.; Baker, J. R., Jr. *Macromolecules* **2002**, *35*, 4510–4520.
(4) Roy, R.; Zanini, D.; Meunier, S. J.; Romanowska, A. *J. Chem. Soc., Chem. Commun.* **1993**, 1869–1872.
(5) Jang, W.-D.; Kataoka, K. *J. Drug Delivery Sci. Technol.* **2005**, *15*, 19–30.
(6) Wiener, E. C.; Brechbiel, M. W.; Brothers, H.; Magin, R. L.; Gansow, O. A.; Tomalia, D. A.; Lauterbur, P. C. *Magn. Reson. Med.* **1994**, *31*, 1–8.
(7) Malik, N.; Evagorou, E. G.; Duncan, R. *Anti-Cancer Drugs* **1999**, *10*, 767–776.
(8) Maruyama-Tabata, H.; Harada, Y.; Matsumura, T.; Satoh, E.; Cui, F.; Iwai, M.; Kita, M.; Hibi, S.; Imanishi, J.; Sawada, T.; Mazda, O. *Gene Ther.* **2000**, *7*, 53–60.

10.1021/cm071451m CCC: $37.00 
Published on Web 10/11/2007

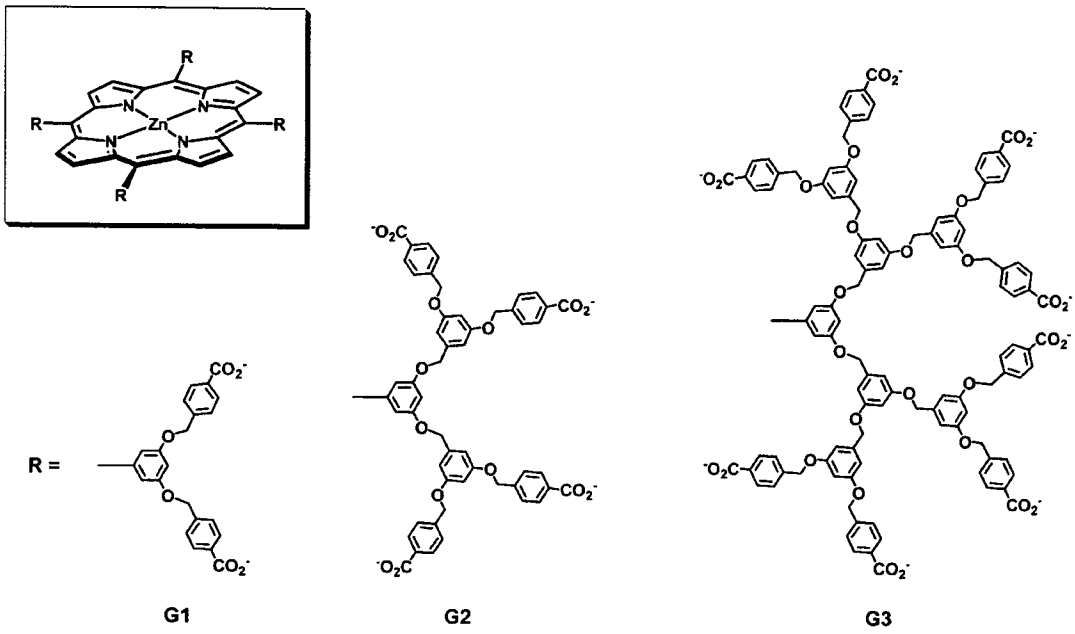


Figure 1. Structures of dendrimer porphyrins (DPs).

Table 1. Physical Properties of DP-Loaded PIC Nanocarriers

| generation | hydrodynamic diameter (nm)[a] | polydispersity index ($\mu_2/\Gamma^2$) | $M_{w,app}$ ($10^5$ g/mol) | association no. PEG-*b*-PLL/DP | CAC[b] (mg/mL) | ζ-potential (mV) |
|---|---|---|---|---|---|---|
| G1 | 126.5 | 0.131 | 2240 | 8989/32585 | <0.1 | 1.11 ± 0.072 |
| G2 | 78.0 | 0.249 | 100 | 399/722 | <0.1 | 0.48 ± 0.31 |
| G3 | 44.0 | 0.030 | 9.26 | 39/38 | <0.1 | −0.20 ± 0.57 |

[a] Cumulant diameter. [b] Critical association concentration.

activation by light at a wavelength matching the absorption wavelength of photosensitizer leads to the generation of reactive oxygen species (ROS) that causes the oxidative destruction of a target tissue.[12,13] As a revolutionary method in preclinical and clinical applications over the last few decades, numerous attempts have been made to improve the PDT efficacy. Among them, the creation of an efficient photosensitizer and its efficient delivery to the target tissue is an attractive topic. An ideal photosensitizer should have the following properties: (1) high quantum yield, (2) a large absorption cross-section, (3) good solubility in an aqueous medium, (4) no dark toxicity, and (5) preferential selectivity to the malignant tissue.[12−15] However, most of the photosensitizers developed in a preclinical or clinical study show poor water solubility with aggregate formation and skin phototoxicity due to a nonspecificity to tumors.[13,16]

On the basis of the above information, we have designed DPs as potential photosensitizers, because we expected that large dendritic wedges can effectively segregate the focal porphyrin cores and thereby prevent collisional quenching of the porphyrins even at a very high concentration.[9−11] In fact, the third generation DPs exhibited a remarkable PDT efficacy. In addition, ionic peripheral functionalities allow the formation of polyioncomplex (PIC) micelles with oppositely charged block copolymers.

In a present study, we investigated the systematic evaluation of the influence of the DP generation on the physicochemical properties and nanocarrier formation. A series of negatively charged DPs (Figure 1; G*n* = *n*-generation dendrimer, $n = 1-3$)[11,17,18] with poly(ethylene glycol)-*block*-poly(L-lysine) (PEG-*b*-PLL)[19−21] were used to form the PIC nanocarriers.

## Results

**Formation of DP-Loaded PIC Nanocarriers.** The DPs were synthesized by a previously reported method.[17] All of the dendrimers were unambiguously characterized by $^1$H NMR and MALDI-TOF-MS measurements. The DPs clearly

(9) Nishiyama, N.; Stapert, H. R.; Zhang, G.-D.; Takasu, D.; Jiang, D.-L.; Nagano, T.; Aida, T.; Kataoka, K. *Bioconjugate Chem.* **2003**, *14*, 58−66.
(10) Zhang, G.-D.; Harada, A.; Nishiyama, N.; Jiang, D.-L.; Koyama, H.; Aida, T.; Kataoka, K. *J. Controlled Release* **2003**, *93*, 141−150.
(11) Jang, W.-D.; Nishiyama, N.; Zhang, G.-D.; Harada, A.; Jiang, D.-L.; Kawauchi, S.; Morimoto, Y.; Kikuchi, M.; Koyama, H.; Aida, T.; Kataoka, K. *Angew. Chem., Int. Ed.* **2005**, *44*, 419−423.
(12) Bonnettt, R. *Chemical Aspects of Photodynamic Therapy*; Gordon and Breach Science Publishers: Amsterdam, 2000.
(13) Pandey, R. K.; Zheng, G. In *The Porphyrin Handbook*; Kadishi, R. K., Smith, K. M., Guilard, R., Eds.; Academic Press: New York, 2000; Vol. 6, pp 157−230.
(14) Derycke Annelies, S. L.; Witte, P. A. M. *Adv. Drug Delivery Rev.* **2004**, *56*, 17−30.
(15) van Dongen, G. A. M. S.; Visser, G. W. M.; Vrouenraets, M. B. *Adv. Drug Delivery Rev.* **2004**, *56*, 31−52.
(16) Hamblin, M. R.; Newman, E. L. *J. Photochem. Photobiol., B* **1994**, *23*, 3−8.
(17) Sadamoto, R.; Tomioka, N.; Aida, T. *J. Am. Chem. Soc.* **1996**, *118*, 3978−3979.
(18) Aida, T.; Jiang, D.-L. In *The Porphyrin Handbook*; Kadishi, R. K., Smith, K. M., Guilard, R., Eds.; Academic Press: New York, 2000; Vol. 3, pp 369−384.
(19) Harada, A.; Kataoka, K. *Macromolecules* **1995**, *28*, 5294−5299.
(20) Harada, A.; Kataoka, K. *Science* **1999**, *283*, 65−67.
(21) Katayose, S.; Kataoka, K. *Bioconjugate Chem.* **1997**, *8*, 702−707.

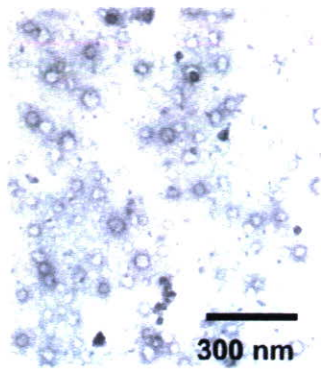


**Figure 2.** TEM images G3-loaded PIC nanocarriers.

formed multimolecular PIC assemblies (PIC nanocarriers) by mixing with PEG-*b*-PLL in aqueous solutions. As shown in Table 1, the DP-loaded PIC nanocarriers have almost neutral $\zeta$-potential values, indicating a charge neutralization between the DPs and PEG-*b*-PLL to form PICs with a PEG palisade. The size and polydispersity index of the PIC nanocarriers, which were evaluated by DLS measurements, strongly depended on the generation number of the DPs (Table 1).[22] The G3-loaded PIC nanocarrier exhibits an average diameter of 44 nm and remarkably low polydispersity index ($\mu_2/\Gamma^2 = 0.030$), which is consistent with the core−shell-type micelle structure. The G2-loaded PIC nanocarrier had an average diameter of 78 nm and remarkably high polydispersity index ($\mu_2/\Gamma^2 = 0.249$), and the G1-loaded PIC nanocarrier showed a relatively large average diameter of 126 nm and a moderate polydispersity index ($\mu_2/\Gamma^2 = 0.131$). Also, the association numbers, apparent molecular weight ($M_{w,app}$), as well as the $\zeta$-potential of the PIC nanocarriers are summarized in Table 1. The G3-loaded PIC nanocarrier was formed from 38 G3 and 39 PEG-*b*-PLL copolymers. The G2-loaded PIC nanocarrier had 1 order of magnitude higher association numbers and $M_{w,app}$ than those of the G3-loaded PIC nanocarrier. The G1-loaded PIC nanocarrier showed much higher association numbers and $M_{w,app}$ values than both the G-2 and the G-3 loaded species. The TEM image of the G3-loaded PIC nanocarriers showed spherical nanoparticles, indicating the formation of a core−shell-type micelle structure (Figure 2).

**Time-Resolved Fluorescence Measurements.** The aggregate formation of photosensitizers results in fluorescence quenching due to an increase in the nonradiative decay of the excited states.[23] Our previous studies[10,11] indicated that large dendritic wedges can successfully prevent the quenching of photosensitizers by steric isolation. In this context, time-resolved fluorescence decay curves of the DPs and DP-loaded PIC nanocarriers were recorded to obtain information about the effect of collisional quenching of the focal porphyrin units within the self-assembled PIC systems. As shown in Figure 3, the free DPs exhibit almost comparable fluorescent decay profiles, indicating that DPs have high solubility in aqueous medium and mostly exist in monomeric

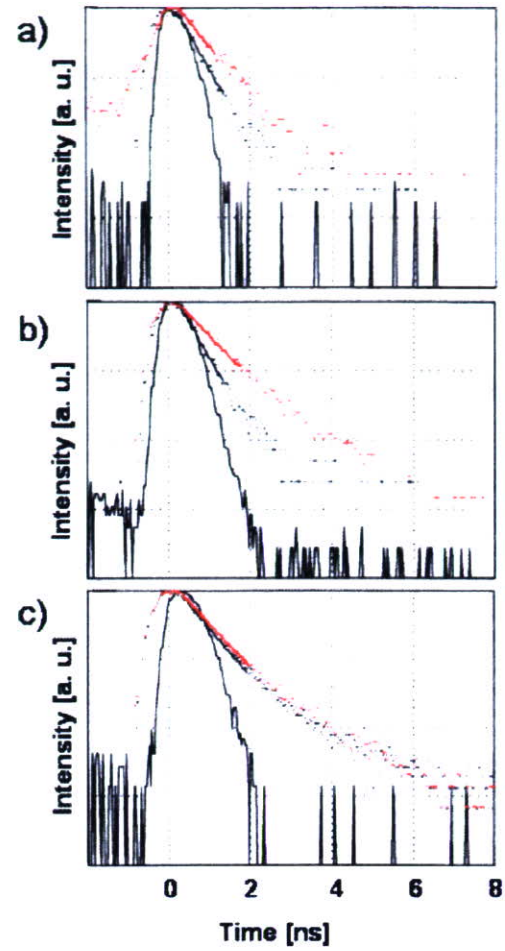


**Figure 3. Fluorescence decay curves of G1 (a), G2 (b), and G3 (c) DPs (red line) and DP-loaded PIC nanocarriers (black line).**

state. Within the PIC nanocarriers, the G1- and G2-loaded PIC nanocarriers exhibit a significant fluorescence quenching signature as compared to the corresponding free DPs. In sharp contrast, the G3-loaded PIC nanocarrier showed almost comparable decay rates to the free G3 (Figure 3c). This result supports our assumption that the large dendritic wedges can prevent the collisional quenching of the photosensitizing units, whereas the relatively small dendritic architecture cannot perfectly prevent the collisional quenching of the focal porphyrin units within the core of PIC nanocarriers.

**Oxygen Consumption Abilities.** The photoinduced oxygen consumption of the DPs and DP-loaded PIC nanocarriers was observed to evaluate the efficiency of the photochemical reactions. Under light irradiation, photosensitizers produce ROS involving singlet oxygen and the superoxide anion. The partial oxygen pressure ($PO_2$) change in the medium containing DPs or PIC nanocarriers with 10% FBS was recorded during photoirradiation. As shown in Figure 4, the G3 and G3-loaded PIC nanocarrier exhibit similar oxygen consumption amounts. In contrast, the oxygen consumption amount appreciably decreased when the G2 or G1 DP was loaded into the nanocarriers. Without 10% FBS, both the DPs and the DP-loaded PIC nanocarriers showed an almost negligible change in the $PO_2$ upon photoirradiation (data not shown),

(22) **Burchard, W.** In *Light Scattering: Principles and Development*; **Brown, W., Ed.; Clarendon Press: New York, 1996.**
(23) **Lakowicz, J. R.** *Principles of Fluorescence Spectroscopy*; **Kluwer Academic/Plenum Publishers: New York, 1999.**

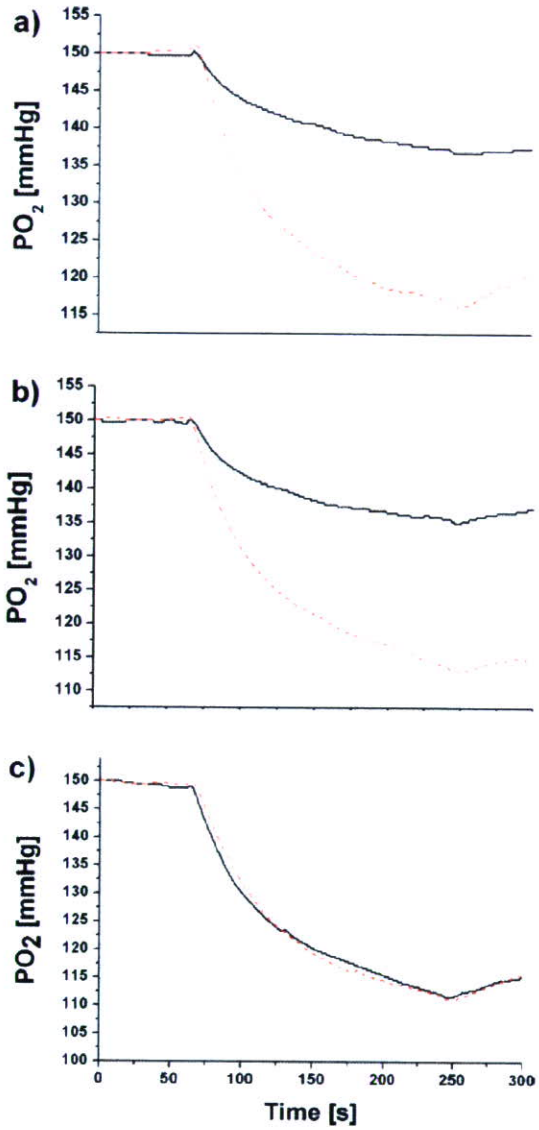


Figure 4. Oxygen partial pressure change of medium included G1 (a), G2 (b), and G3 (c) DPs (– – –) and DP-loaded PIC nanocarriers (–).

indicating that the proteins in FBS act as sacrificial acceptors of ROS.

**Cellular Uptake.** Efficient cellular association of a photosensitizer could lead to a high PDT efficacy. To quantitatively evaluate the cellular uptake of DPs and DP-loaded PIC nanocarriers, HeLa cells were incubated with 6.25 $\mu$M DPs or DP-loaded PIC nanocarriers having an equivalent amount of DPs (Figure 5). The cellular uptake of DPs is significantly enhanced by the incorporation into nanocarriers, indicating that the anionic surface of the DPs results in a limited interaction with a negatively charged cellular membrane. Charge neutralization and shielding of the PICs by the PEG segment might reduce the electrostatic repulsion with a cell. Therefore, encapsulation of the DPs into the PIC nanocarriers might be effective for the intracellular delivery of DPs.

The uptake amount of DPs showed a strong generation dependence. Interestingly, the G1-loaded PIC nanocarrier shows the largest uptake amount, while the G3-loaded PIC

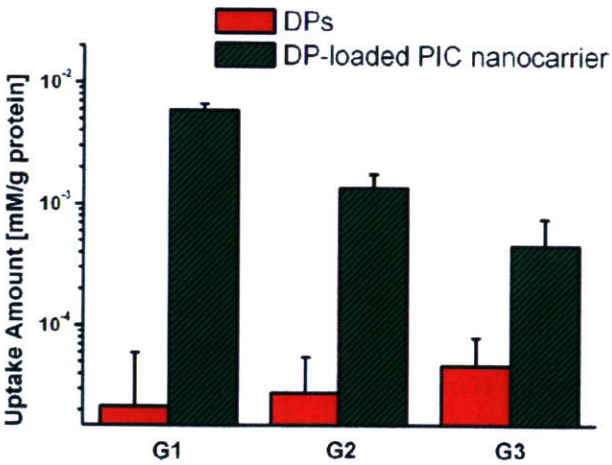


Figure 5. Cellular uptake amount of DPs and DP-loaded PIC nanocarriers. 6 $\mu$M DPs or DP-loaded PIC nanocarriers with equivalent amount of DPs is incubated.

nanocarrier gave the lowest uptake amount among the three DP-loaded PIC nanocarriers. The difference in the cellular uptake between generations is possibly caused from the morphological difference in the nanocarriers, such as the size, association number, and stability of the PICs.

**Photodynamic Effect.** The in vitro photodynamic effect against HeLa cells was evaluated by the MTT assay. The DPs and the DP-loaded PIC nanocarriers showed an almost negligible cytotoxicity under dark conditions (data not shown), whereas each species exhibited a strong photocytotoxicity. Figure 6 shows the cell viability−concentration curve, where the DPs apparently exhibit a remarkable increase in the photocytotoxicity by incorporation into the nanocarriers. Fifty percent inhibitory concentrations ($IC_{50}$) of the DPs and DP-loaded PIC nanocarriers, the concentration of photosensitizer at which 50% mortality of tumor cells as compared to the control was observed after a photoirradiation, were calculated from the cell viability−concentration curve (Table 2). The G1- and G2-loaded PIC nanocarriers exhibited 7.5 and 50 times, respectively, higher photocytotoxicities as compared to the G1 and G2 DPs. Notably, the G3-loaded PIC showed a 167 times enhanced photocytotoxicity as compared to free G3 DP.

## Discussion

All of the DPs showed high solubility in aqueous medium due to the ionic charges of dendritic wedges. When the DPs are mixed with PEG-*b*-PLL copolymers in a stoichiometric ratio, positively charged PLL segments successfully interact with negative surface functionalities of DPs to form the DP-loaded PIC nanocarriers. The values of the $\zeta$-potential also well coincide with the charge neutralization between the DPs and PEG-*b*-PLL as well as encapsulation of the PICs within the PEG layer.

Notably, the PIC nanocarriers had a high stability upon dilution with a very low critical association concentration being observed. These features are significantly important parameters from a therapeutic point of view. For target delivery of the therapeutic agent, the drug formulation should have a tolerance against dilution and maintain long circula-

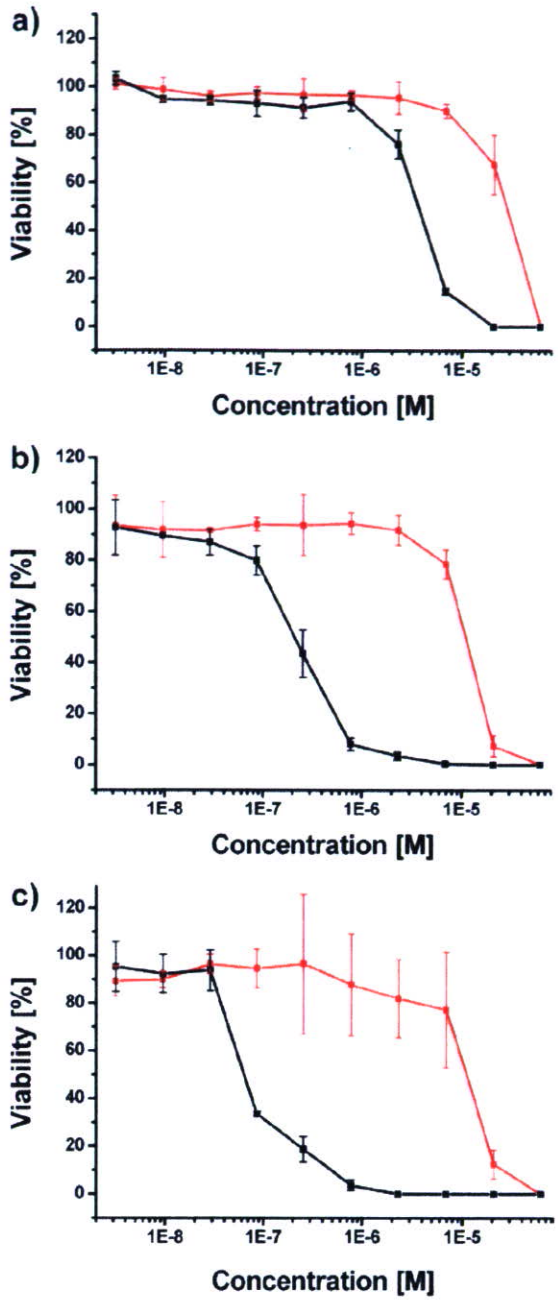


**Figure 6.** The viability of Hela cells treated with G1 (a), G2 (b), and G3 (c) DPs (red line) and DP-loaded PIC nanocarriers (black line).

**Table 2. $IC_{50}$ of DPs and DP-Loaded PIC Nanocarriers (unit: M)**

| generation | DP | DP-loaded PIC nanocarrier |
|---|---|---|
| G1 | $3.0 \times 10^{-05}$ | $4.0 \times 10^{-06}$ |
| G2 | $1.2 \times 10^{-05}$ | $2.0 \times 10^{-07}$ |
| G3 | $1.0 \times 10^{-05}$ | $6.0 \times 10^{-08}$ |

tion times in the blood stream. Also, the PIC nanocarriers may facilitate targeting to tumor tissues by the so-called enhanced permeability and retention (EPR) effect.[24]

The DLS measurement of the DP-loaded PIC nanocarriers exhibited a generation dependence, where the G3-loaded PIC nanocarrier showed a nicely dispersed particle formation with a diameter of 44 nm. The sizes of the G1- and G2-loaded PIC nanocarriers are generally larger than that of the G3-loaded PIC nanocarrier. TEM observations of the G3-loaded PIC nanocarrier showed a spherical assembly formation, which is consistent with the core−shell-type micelle structure. In contrast, the G2- or G1-loaded PIC nanocarrier showed a high polydispersity. The difference in size and distribution might be attributable to the number of anionic charges and dendritic architecture. The relatively open architecture of the G1 and G2 cannot perfectly prevent $\pi-\pi$ interactions among the porphyrin cores when they form the PICs. Thus, the association of the DPs with a low generation is possibly driven by the $\pi-\pi$ interaction as well as an electrostatic interaction.

In the photodynamic process sequence, the DPs are converted to excited state under light irradiation, and then they transfer excited energy or electrons to oxygen molecules to generate the ROS. The time-resolved fluorescence observation provides information about the energy transduction procedure, and the oxygen consumption ability is directly related to the ROS generation. The fluorescence decay and oxygen consumption profiles of each DP did not have large differences among the differnet generation of DPs (Figures 3 and 4). Also, the cellular uptake and photocytotoxicity of DPs were almost comparable values regardless of the generation of DPs (Figures 5 and 6). A molecular aggregation of the photosensitizers might result in the fluorescence quenching behavior. All of the free DPs exhibit almost comparable fluorescence decay profiles, indicating that DPs are succesfully segregated within aqueous medium due to high solubility and charge repulsion of surface carboxylic acid functionalities. On the other hand, the G1 and G2 showed a significant fluorescence quenching by incorporation into the PIC nanocarriers (Figure 3), indicating that the G1 and G2 have high proportions of nonradiative decays within the PIC nanocarriers by collisional quenching. Also, the G1- or G2-loaded PIC nanocarriers exhibited a significant decrease in their oxygen consumption ability as compared to the free DPs (Figure 4). We noted that either the DPs or the DP-loaded PIC nanocarrier solution without 10% FBS showed almost negligible changes in the $PO_2$ upon photoirradiation, indicating that the proteins in FBS act as sacrificial acceptors of the ROS. In other words, if proteins do not exist in the medium, once generated, the ROS promptly revert to the ground-state oxygen molecules due to their short lifetimes. This fact means that the reduced oxygen consumption of the G1- or G2-loaded PIC nanocarrier is possibly caused by the increase in the nonradiative decays of the excited states and also the generation of less reactive ROS. Additionally, the diffusivity of oxygen molecules is possibly reduced within the G1- and G2-loaded PIC nanocarriers due to their large hydrodynamic size. In contrast, the G3-loaded PIC nanocarrier showed an almost comparable fluorescence decay profile (Figure 3) and oxygen consumption to the free G3 (Figure 4), indicating that the third generation dendritic wedges can sufficiently prevent aggregation of the photosensitizing porphyrin units, and the G3 can efficiently transfer excited energy to oxygen molecules without loss even in a highly concentrated state of G3 in the PIC nanocarrier. Also,

(24) Maeda, H.; Wu, J.; Sawa, T.; Matsumura, Y.; Hori, K. *J. Controlled Release* **2000**, *65*, 271−284.

**Table 3. The Change of Parameters of DPs by Inclusion into the PIC Nanocarriers in Each Generation System**

| generation | fluorescence lifetime | oxygen consumption | uptake ratio (*A*) | photocytotoxicity ratio (*B*) | *B*/*A* |
|---|---|---|---|---|---|
| G1 | shortened | decreased | 95 | 7.5 | 0.079 |
| G2 | shortened | decreased | 53 | 50 | 0.94 |
| G3 | maintained | no change | 15 | 167 | 11.1 |

the ROS generated from the G3-loaded PIC nanocarrier can efficiently react with serum proteins in the media.

Positively charged particles might have a large affinity against cell membranes, but the cationic particles easily associate with the negatively charged serum proteins such as albumin. Therefore, DPs with an anionic periphery may have a high availability from a clinical point of view as compared to the positively charged ones. Furthermore, the formation of the PIC nanocarriers may prevent aggregate formation during the blood circulation due to the steric stabilization of the PEG shell layer. Also, the formation of the PIC nanocarriers may improve the uptake amount of the DPs by the charge neutralization. In fact, DP-loaded PIC nanocarriers showed an appreciably high level of uptake as compared to the free DPs (Figure 5). Correspondingly, the photocytotoxicity of each PIC nanocarrier was remarkably improved as compared to that of the free DPs (Figure 6). One of the interesting aspects in this regard is the enhanced photocytotoxicity of the PIC nanocarriers encapsulating DP with an increased generation despite the generation-dependent relative decrease in their uptake amount of PIC nanocarriers.

To evaluate the effect of the DP generations on the PDT efficacy, various parameter changes after the incorporation of the DPs into the PIC nanocarriers are summarized in Table 3. The cellular uptake and photocytotoxicity ratios are obtained by normalization of the cellular uptake amount and the $IC_{50}$ of the DP-loaded PIC nanocarriers by those of the free DPs. Additionally, the photocytotoxicity ratio is normalized by the uptake ratio for calculating the PDT efficacy of the individual DPs (*B*/*A*). G1 shows the reduced PDT efficacy by incorporation into the PIC nanocarriers. This is consistent with the shortened lifetime and decreased oxygen consumption of the G1-loaded PIC nanocarrier. However, the G2-loaded PIC nanocarrier exhibits a comparable PDT efficacy with the free G2 despite the shortened fluorescent lifetime and decreased oxygen consumption. Notably, the incorporation of the G3 into the PIC nanocarrier shows an 11-fold enhancement of the PDT efficacy. The high local concentration of DPs within the core of PIC nanocarrier is able to generate a large amount of ROS at a local site, which may lead to a high photochemical oxidation level and easily overcome the photodynamic threshold. Also, there is a possibility to change the subcellular localization of DPs by the formation of PIC nanocarriers. It should be noted in this regard that the pegylated chlorin-e6 as well as the PEG-based polymeric micelles were recently reported to show an enhanced localization in several cytoplasmic organelles including the mitochondria.[25,26] Now, we are going to observe the subcellular localization of the DPs to investigate detailed mechanism of the enhanced PDT efficacy.

Consequently, in the present investigation, we were able to determine that the PDT efficacy is highly dependent on the generation of the DPs when they formed PIC nanocarriers. The PIC nanocarriers formed from large DPs produced a high quantum yield of ROS generation and a strong nanocarrier effect, resulting in a high PDT efficacy.[27]

## Conclusions

This study was conducted to systematically investigate the effect of the dendritic structures of DPs on the physicochemical property, cellular uptake, and PDT efficacy. A dendrimer generation-dependent PDT efficacy was revealed by the inclusion of DPs into supramolecular nanocarriers of PICs. To summarize the results in the present Article, we can consider the following several parameters to design effective photosensitizers: (1) Large dendritic wedges form uniform core−shell PIC micelles. (2) PIC nanocarrier formation enhances cellular uptake. (3) Incorporation of DPs in nanocarrier systems may provide enhancement of the photodynamic efficacy. In this way, G3 with a large dendritic structure encapsulated into the PIC micelles would be an ideal photosensitizer and may have a high utility for in vivo PDT applications.

**Acknowledgment.** This study was supported by the Industrial Technology Research Grant Program in '04 from the New Energy and Industrial Technology Development Organization (NEDO) of Japan. Y.L. acknowledges the JSPS Young Scientist Fellowship.

**Supporting Information Available:** Materials and detailed experimental procedures (PDF). This material is available free of charge via the Internet at http://pubs.acs.org.

CM071451M

(25) Hamblin, M. R.; Miller, J. L.; Rizvi, I.; Ortel, B.; Maytin, E. V.; Hasan, T. *Cancer Res.* **2001**, *61*, 7155−7162.
(26) Savic, R.; Luo, L.; Eisenberg, A.; Maysinger, D. *Science* **2003**, *300*, 615−618.
(27) Ideta, R.; Tasaka, F.; Jang, W.-D.; Nishiyama, N.; Zhang, G.-D.; Harada, A.; Yanagi, Y.; Tamaki, Y.; Aida, T.; Kataoka, K. *Nano Lett.* **2005**, *5*, 2426−2431.

Available online at www.sciencedirect.com
ScienceDirect
Biomaterials 28 (2007) 5169 5175
Biomaterials
www.elsevier.com/locate/biomaterials

# Gene delivery with biocompatible cationic polymer: Pharmacogenomic analysis on cell bioactivity

Kayo Masago[a,1], Keiji Itaka[a,1], Nobuhiro Nishiyama[a], Ung-il Chung[a,c,d], Kazunori Kataoka[a,b,d,*]

[a]*Division of Clinical Biotechnology, Center for Disease Biology and Integrative Medicine, Graduate School of Medicine, The University of Tokyo, Japan*
[b]*Department of Materials Science and Engineering, Graduate School of Engineering, The University of Tokyo, Japan*
[c]*Department of Bioengineering, Graduate School of Engineering, The University of Tokyo, Japan*
[d]*Center for Nanobio Integration, The University of Tokyo, 7-3-1 Hongo, Bunkyo-ku, Tokyo 113-0033, Japan*

Received 7 June 2007; accepted 10 July 2007
Available online 30 July 2007

**Abstract**

The availability of non-viral gene delivery systems is determined by their capacity and safety during gene introduction. In this study, the safety issues of polyplex were analyzed from the standpoint of the biomolecular mechanisms. P[Asp(DET)], a newly developed polymer, polyasparagine carrying the *N*-(2-aminoethyl)aminoethyl group as the side chain which was recently revealed to show good transfection efficiency to primary cells, was compared to conventional linear poly(ethylenimine) (LPEI). After transfection toward a bioluminescent cell line, P[Asp(DET)] maintained the expression level of stably expressing luciferase. In contrast, LPEI showed a decrease in the luciferase expression, while the similar expression of exogenous reporter gene was obtained. Evaluation of the housekeeping genes expression as well as the profiles of pDNA uptake after transfection suggested the time-dependent toxicity of LPEI that perturbs cellular homeostasis. Consistently, the induction of osteogenic differentiation by functional gene introduction was achieved only by P[Asp(DET)], even though appreciable expression of the gene was achieved by LPEI. It is crucial that this aspect of safety be taken into account, especially when the gene introduction is applied to primary cells to regulate such cell function as differentiation. This biomolecular analysis focusing on cellular homeostasis is beneficial for assessing the practicability of the gene delivery systems for clinical application.


*Keywords:* Biocompatibility; Gene transfer; Cationic polymer; Cytotoxicity; Cell differentiation

## 1. Introduction

Gene therapies have attracted progressive attention for the treatment of numerous intractable diseases, but the lack of safe and efficient gene-delivery systems is an obstacle to their clinical application. Viral vectors are known to be highly potent gene delivery systems, yet may also induce adverse side effects, including severe immunological and toxicological responses. In fact, recent clinical trials using viral vectors have been halted due to unprecedented toxicity, including the death of a patient [1–4]. Therefore, non-viral gene carriers such as cationic lipids and polymers are expected to be an alternative to viral vectors directing therapeutic genes to target tissues.

The availability of gene carriers is largely determined by their transfection efficiency and cytotoxicity. Although the latter is generally evaluated through the viability assay of cultured cells such as an MTT assay [5], an MTT assay only reflects the non-specific outcome of cell death. Synthetic carriers may induce side effects including complement activation, carcinogenicity, teratogenicity and immunogenicity, all of which are serious concerns for clinical application [6]. Thus, the safety issues of non-viral gene carriers, both on a cellular and systemic basis,

*Corresponding author. Department of Materials Engineering, Graduate School of Engineering, The University of Tokyo, 7-3-1 Hongo, Bunkyo-ku, Tokyo 113-0033, Japan. Tel.: +81 3 5841 7138; fax: +81 3 5841 7139.
*E-mail address:* kataoka@bmw.t.u-tokyo.ac.jp (K. Kataoka).
[1]These authors contributed equally to this work.

0142-9612/$ - see front matter © 2007 Elsevier Ltd. All rights reserved.
doi:10.1016/j.biomaterials.2007.07.019

are critical for their clinical development, requiring careful analysis of the toxicity by exploring the biomolecular mechanisms. In this regard, a pharmacogenomic analysis of the global gene expression in the transfected cells is of particular interest. This approach has recently been advocated as polymer genomics or material genomics, and several studies have been reported to have applied it for the evaluation of non-viral gene carriers [7,8].

Recently, we developed a novel block catiomer-based gene delivery system that showed excellent capacity for *in vitro* transfection to primary cells [9]. This system is composed of plasmid DNA (pDNA) and poly(ethyleneglycol)-block-polyasparagine carrying the *N*-(2-aminoethyl) aminoethyl group $(CH_2)_2NH(CH_2)_2NH_2$ as the side chain (PEG-PAsp[DET]). Ethylene diamine units located at the side chain are only half protonated under neutral pH and are thus feasible candidates to perform the so-called proton sponge effect, which has been believed to be the major mechanism for the excellent transfection efficiency of some polyamine derivatives having substantially lowered pKa such as poly(ethylenimine) (PEI) [10–12]. As well as the good transfection efficiency, the polyplex micelles from this block catiomer showed minimal cytotoxicity toward various primary cells, achieving the successful *in vivo* gene introduction to the vascular lesions [13] and the effective induction of cell differentiation both *in vitro* and *in vivo* through the effective expression of the genes encoding transcriptional factors [14].

These results motivated us to perform an additional toxicogenomic study of P[Asp(DET)] in order to ensure the safety for future clinical application. Linear PEI (LPEI) was used as a control, representing the common polycation for the construction of polyplexes. Although P[Asp(DET)] and LPEI both have a buffering capacity under an endosomal pH, they showed a considerable difference in the toxicological profiles which revealed the appreciably lowered toxicity of the former compared to the latter. In particular, the time-dependent change in the pharmacogenomical toxicity toward the targeted cells was evaluated in detail, in regards to the capacity of inducing cell differentiation through the transfection of functional genes encoded in the encapsulated pDNA in the polyplex.

## 2. Materials and methods

### 2.1. Materials

pGL3-control pDNA encoding firefly luciferase (Promega, Madison, WI, USA), pRL-CMV pDNA encoding renilla luciferase (RL) (Promega), and EGFP-C1 pDNA encoding EGFP (Clontech, Palo Alto, CA, USA) were amplified in the *Escherichia coli* strain DH5α, which was isolated and purified using a QIAGEN HiSpeed Plasmid Maxi Kit (Qiagen, Hilden, Germany). pCMV5 pDNA expressing HA-tagged mouse caALK6 and pcDEF3 pDNA expressing Flag-tagged mouse Runx2 were generous gifts from Dr. M. Krüppel (Mt. Sinai Hospital, Toronto, ON, Canada) and Dr. K. Miyazono (University of Tokyo, Tokyo, Japan), respectively. The concentration of DNA was determined by measuring the UV absorption at 260 nm.

### 2.2. Cells

HuH-7 cells were obtained from the Riken Cell Bank (Tsukuba, Japan). Bioluminescent cells (HuH-7-luc) stably expressing firefly luciferase were kindly provided by Mr. S. Matsumoto (University of Tokyo). Dulbecco's modified Eagle's medium (DMEM) and fetal bovine serum (FBS) were purchased from Sigma-Aldrich (St. Louis, MO, USA).

### 2.3. Polycations for the preparation of polyplex

LPEI (Exgen 500, $M_w$ = 22 kDa) was purchased from MBI Fermentas (Burlington, ON, Canada). Diethylenetriamine (DET) was purchased from Tokyo Kasei Kogyo (Tokyo, Japan). All other chemicals were purchased from Wako Pure Chemical Industries (Osaka, Japan). P[Asp(DET)] was synthesized by the side-chain aminolysis reaction of the poly (β-benzyl L-aspartate) (PBLA) as previously reported [9]. Briefly, the PBLA was synthesized by the ring-opening polymerization of the β-benzyl-L-aspartate *N*-carboxyanhydride (BLA-NCA) initiated by the primary amine of *n*-butylamine in *N,N*-dimethylformamide (DMF)/dichloromethane (1:10) at 40 °C, followed by the acetylation of the *N*-terminal amine with acetic anhydride. Gel permeation chromatography (GPC) was performed to confirm a unimodal molecular weight distribution ($M_w/M_n$ 1.20) of PBLA by TOSHO HLC-8220 (columns: TSK-gel G4000HHR + G3000HHR, eluent: DMF + 10 mM LiCl, $T$ = 40 °C, detector: refractive index). The degree of polymerization of PBLA was determined as 98 from the $^1$H NMR spectrum (JEOL EX300 spectrometer: JEOL, Tokyo, Japan). Then, the side-chain aminolysis reaction of PBLA was performed by mixing the DMF solution of PBLA(50 mg/ml) with a 50-fold excess of DET in DMF at 40 °C to obtain P[Asp(DET)].

### 2.4. Polyplex formation

Each polyplex sample with a pDNA concentration of 33 μg/mL was prepared by simply mixing pDNA and polycation(LPEI or P[Asp(DET)]) at the indicated *N/P* ratio ( = [total amines in polycation]/[DNA phosphates]) in a 10 mM Tris HCl (pH 7.4) buffer solution.

### 2.5. Dual luciferase measurement on HuH-7-luc cells transfected with pRL-CMV pDNA

HuH-7-luc cells were seeded on 96-well culture plates ($3 \times 10^3$ cells/well) and incubated overnight in 100 μl DMEM supplemented with 10% FBS and penicillin/streptomycin. After the culture medium was replaced with fresh medium containing 10% FBS, 5.5 μl of the polyplexes composed of P[Asp(DET)] or LPEI (final DNA concentration: 33 μg/ml) were applied to each well. After 24 h, the medium was changed to remove the polyplexes, followed by further incubation for 24 or 48 h. The firefly and RL activities were measured using a Dual-Luciferase Reporter Assay System (Promega) according to the protocol provided by the manufacturer, using a GloMax™ 96 Microplate Luminometer (Promega).

### 2.6. Cell proliferation assay

HuH-7-luc cells ($6 \times 10^4$ cells/well) were seeded in six-well plates and cultured overnight. After the transfection as described above (polyplex solution: 90 μl/well), the cells were washed with phosphate-buffered saline (PBS), trypsinized, and scraped off. Then the cell number was counted by a nucleo counter (Chemometec, Tokyo, JAPAN) following the protocol provided by the manufacturer. The measurement was duplicated.

### 2.7. Lactate dehydrogenase (LDH) assay

The degree of membrane destabilization was examined by lactate dehydrogenase (LDH) activity liberated from the cytoplasm. The cells were plated on 96-well plates and incubated overnight in 100 μl of DMEM

containing 10% FBS. Then the medium was changed and 5.5 μl of polyplex was added to each well similarly as in the transfection described above. After 4, 8, or 24 h, the plates were centrifuged for 5 min at 110*g*. Then, 50 μl of aliquots in each well were collected and subjected to the LDH measurement. A CytoTox 96 Non-Radioactive Cytotoxicity Assay kit (Promega) was used following the protocol provided by the manufacturer, using a plate reader AD200 (Beckman Coulter, Inc., USA) for reading the OD at 490 nm to determine the amount of the produced diformazan. Freeze-chaw cells were used to calibrate 100% LDH activity. To compare the cytotoxicity between P[Asp(DET)] and LPEI, the parametrical analysis using the Student's *t*-test was performed.

### 2.8. Quantitative assay on the cellular uptake of pDNA by real-time quantitative PCR

EGFP-C1 pDNA expressing EGFP was transfected to HuH-7. $8 \times 10^4$ HuH-7 cells/well were plated in six-well plates and cultured overnight, and then the transfection was done similarly as described before. At the indicated time periods (4, 8 and 24 h), the DNA was collected and purified from each well using a Wizard Genomic DNA purification Kit (Promega), then subjected to the PCR for the quantification of pDNA copies encoding EGFP. The copy number of β-actin (βA) was also determined by the ABI 7500 Fast Real-Time PCR systems to normalize the cell number (Applied Biosystems, Foster City, CA, USA). The sequences of the primers and probe used for EGFP were as follows: forward primer GGGCACAAGCTGGAGTACAAC and reverse primer TCTGCTT GTCGGCCATGATA. The sequence of the probe was ACAGCCA CAACGTCT with FAM as a fluorescent dye on the 5-end and MGB as a fluorescence quencher dye labeled on the 3-end. For βA amplification and quantitation, the forward and reverse primers and probe were purchased as a standard TaqMan gene expression assay kit from Applied Biosystems. PCR was done for 20 s at 95 °C, followed by 3 s at 95 °C and 60 s at 60 °C for 40 cycles. A linear relationship between the number of cells and threshold cycle for the βA gene amplification was confirmed (data not shown).

### 2.9. Evaluation of osteocalcin mRNA expression

Osteogenic differentiation of the mouse calvarial cells was evaluated by the expression of osteocalcin mRNA, an osteoblast-differentiation marker. Mouse calvarial cells were isolated from the calvariae of neonatal littermates. The experimental procedures were handled in accordance with the guidelines of the Animal Committee of the University of Tokyo. Calvariae were digested for 10 min at 37 8 °C in an enzyme solution containing 0.1% collagenase and 0.2% dispase for five cycles. Cells isolated by the final four digestions were combined and cultured in DMEM supplemented with 10% FBS and penicillin/streptomycin. For induction of the differentiation assays, $3 \times 10^4$ primary mouse calvarial cells were plated in six-well culture plates and cultured for 24 h. After changing the medium to that containing 10% FBS and dexamethazone, polyplexes containing pDNAs expressing caALK6 and Runx2 were applied to each well by a similar transfection procedure as that previously described. The culture medium was refreshed on Day 3 after transfection, then changed every 3 days. On Days 5 and 11, the cells were washed with PBS and the total RNA was collected using the RNeasy Mini Preparation Kit (Qiagen) according to the manufacturer's protocol. Gene expression was analyzed by a quantitative PCR. 500 ng of total RNA was analyzed in a final volume of 50 μl. Reverse transcription was performed for 30 min at 50 °C followed by PCR: 50 °C for 2 min, 95 °C for 10 min, followed by 40 cycles of 95 °C for 15 s and 60 °C for 1 min using the Quantitect SYBR Green PCR Kit (Qiagen). Each mRNA expression was normalized to levels of mouse βA mRNA. The primers used were as follows: osteocalcin: forward primer (AAGCAGGAGGGCAATAAGGT) and reverse primer (TTTGTAGGCGGTCTTCAAGC); mouse βA: forward primer (AGATGTGGATCAGCAAGCAG), reverse primer (GCGCAAGT-TAGGTTTTGTCA). To compare the osteocalcin expressions using P[Asp(DET)] or LPEI, the parametrical analysis using the Student's *t*-test was performed.

### 2.10. Housekeeping gene expression assay

After a similar transfection procedure as previously described was performed, the total RNA was collected at 24 or 72 h. To evaluate the expressions of the housekeeping genes, a Taqman Human Endogenous Control Plate (Applied Biosystems) was used according to the manufacturer's protocol, including 18S rRNA, acidic ribosomal protein (PO), βA, cyclophilin (CYC), glyceraldehyde-3-phosphate dehydrogenase (GAPDH), phosphoglycero-kinase (PGK), β2-microglobulin (β2m), β-glucronidase (GUS), hypoxanthine ribosyl transferase (HPRT), TATA binding protein (TBP) and transferrin receptor (TfR). The control cells serve as a baseline for the assays and are shown as zero on the graph. The results are expressed in the comparative cycle threshold; $\Delta C_T$, greater than or less than the control $\Delta C_T$.

## 3. Results and discussion

### 3.1. In vitro transfection toward bioluminescent cell line

The bioluminescent human hepatoma cell line (HuH-7-Luc) stably expressing firefly luciferase (Luc) was used to evaluate the pharmacogenomic influence as well as the transfection efficiency of the polyplexes. After the transfection of RL using P[Asp(DET)] or LPEI, both the Luc and RL expressions were estimated simultaneously. The expressions were normalized by the number of cells, which were directly counted after scraping the cells from the culture plates.

The exogenous RL expressions per cell in Fig. 1(a) showed that the P[Asp(DET)] polyplex had comparable transfection efficiency to the LPEI polyplex giving the highest expression at 48 h after transfection. In contrast, the endogenous Luc expression showed a different profile between the two polyplexes; the Luc expression of the cells transfected by the P[Asp(DET)] polyplex was equivalent as that of the control cells, while the cells transfected by the LPEI polyplex showed a gradual decrease in Luc expression per cell (Fig. 1(b)). The cell numbers shown in Fig. 1(c) revealed that the proliferation was significantly inhibited by the transfection using LPEI after Day 2, compared to that of the other two groups (the cells transfected by P[Asp(DET)] and the control). Note that in these experiments, the polyplexes in the medium were removed at 24 h after transfection by changing the culture medium. Thus, these results suggest that although the exogenous RL gene expression showed an increase until Day 2, the internalized LPEI into the target cells by Day 1 had some continuous inhibiting effects on the proliferation and endogenous gene expression in the targeted cells. It is reasonable to assume that the LPEI released from the polyplex may impair the intracellular activities in a time-dependent manner.

### 3.2. Investigation of the cytotoxicity induced by LPEI

To investigate the detailed mechanisms of the time-dependent cytotoxicity possibly induced by LPEI, we

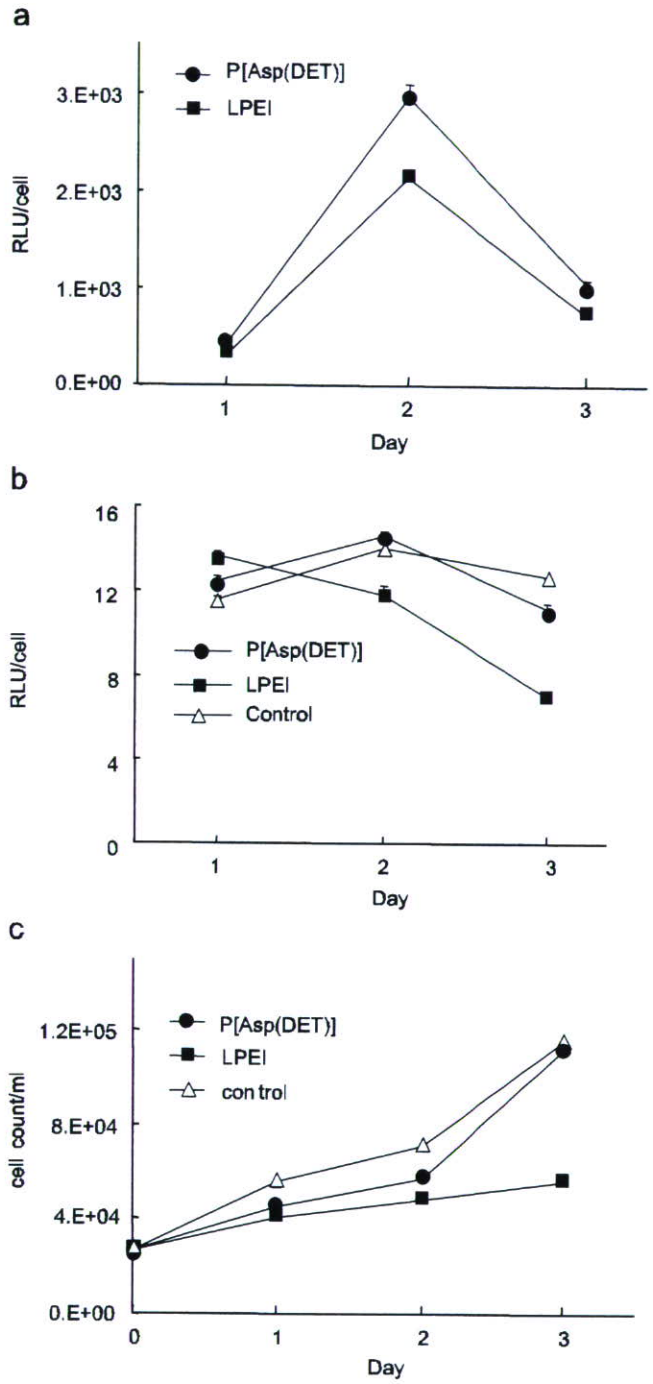


Fig. 1. *In vitro* transfection toward HuH-7-Luc cells. (a) Exogenous renilla luciferase expression. (b) Endogenous firefly luciferase expression. (c) Cell proliferation assay. Transfection was performed by P[Asp(DET)] (closed circle) or LPEI (closed square) polyplexes formed at $N/P = 10$. Gene expression was evaluated for 3 days after transfection and normalized by the cell number. Each data of gene expression represents mean ± SD ($n = 8$). The data of cell number are means ($n = 2$).

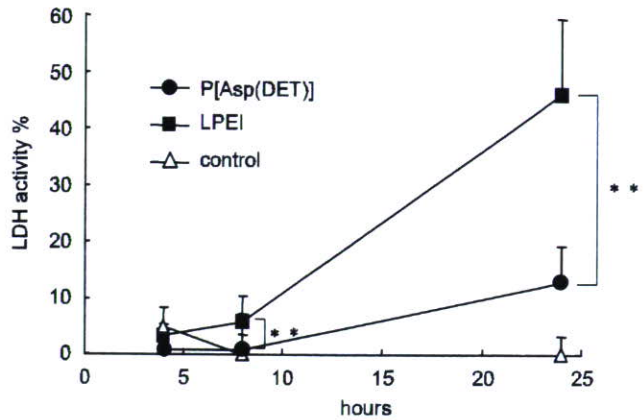


Fig. 2. Evaluation of LDH activity after transfecton using P[Asp(DET)] (closed circle) or LPEI (closed square) polyplexes. Each data represents mean ± SD ($n = 8$). Freeze-chaw cells were used to calibrate 100% LDH activity. $^{**}P<0.01$.

further assessed each step involved in the transfection process. The first step is apparently the cellular association and internalization of the gene carriers. It is assumed that these events may evoke membrane destabilization, possibly causing cytotoxic effects [15]. The change in membrane permeability due to the interaction with the polyplexes was examined by an LDH assay under the same condition as used in the transfection experiments above. As presented in Fig. 2, the cells transfected by the LPEI polyplex revealed a time-dependent increase in the leakage of LDH until 24 h after transfection. In contrast, the P[Asp(DET)] polyplex induced a minimal LDH leakage compared to the control. Considering the similar cationic nature of LPEI and P[Asp(DET)], the membrane destabilization after their association onto the plasma membrane is expected to be similar, which is apparently not the case observed here. The discrepancy between the two polymers on the time-dependent LDH leakage suggests that factors other than simple electrostatic interaction play a substantial role in the process of membrane destabilization.

The uptake amount of reporter gene into the HuH-7 cells by the P[Asp(DET)] or LPEI polyplex was determined by a real-time PCR in terms of gene copies per cell from the total DNA samples [16–18]. As seen in Fig. 3(a), the uptake amount of reporter gene showed a continuous increase until 24 h after the transfection in the case of the P[Asp(DET)] polyplex. The amount of reporter genes internalized with the LPEI polyplex was similar to that with the P[Asp(DET)] polyplex at 8 h, yet was significantly reduced by extending the transfection time to 24 h. One possible reason for this phenomenon might be the rapid dissociation of pDNA from LPEI in the cytoplasm as reported in the literature [19], resulting in its fast degradation by cytoplasmic enzymes [20,21]. However, when the culture medium was changed to remove the polyplexes at 4 h after the transfection, both systems showed a similar profile of a gradual decrease in the copy number after the medium change (Fig. 3(b)), suggesting the similar stability of the internalized pDNAs for both systems. These results suggest that the decrease in the internalized amount of the reporter gene with the LPEI polyplex shown in Fig. 3(a) may be due to